University of Warsaw
Faculty of Mathematics, Informatics and Mechanics

Jan Poleszczuk

Exploring potential tumour growth modulating mechanisms in cells having different status of TP53 gene

doctoral thesis

Supervisor

dr hab. Urszula Foryś

Institute of Applied Mathematics
University of Warsaw

Co-supervisor

dr hab. n. med. Maria Wideł

Faculty of Automatic Control, Electronics and Computer Science
Silesian University of Technology

September 2015

Oświadczenie autora rozprawy:
oświadczam, że niniejsza rozprawa została napisana przeze mnie samodzielnie.

September 30, 2015 . . . . . .
data *Jan Poleszczuk*

Oświadczenie promotora rozprawy:
niniejsza rozprawa jest gotowa do oceny przez recenzentów.

September 30, 2015 . . . . . .
data *dr hab. Urszula Foryś*

Oświadczenie kopromotora rozprawy:
niniejsza rozprawa jest gotowa do oceny przez recenzentów.

September 30, 2015 . . . . . .
data *dr hab. n. med. Maria Wideł*

...

Contents

Chapter 1

Introduction

1.1 Motivation

It is estimated that approximately 14.1 million new cancer cases were diagnosed worldwide in 2012 alone, from which about 1 million in Central and Eastern Europe [123], see Fig. 1.1. The estimates for cancer related deaths worldwide in 2012 provide a shocking number of 8.2 million cases [123] – that is more or less the current population of Switzerland. In Poland there were about 140 thousand new cases of malignant tumors in 2010, which is more than twice as much as in the year 1980 [31]. In the same year 2010 there were about 93 thousand registered cancer associated deaths in Poland, making cancer the second leading cause of death, just after heart diseases [31]. Cancer became a major public health concern in most of the parts of the world and in a few years it might become a leading cause of death in the United States, surpassing heart diseases [105]. The most frequently diagnosed cancers worldwide are breast among females ($\approx$ 1.7 mln new cases in 2012) and cancers of respiratory system among males ($\approx$ 1.2 mln new cases in 2012), with an estimated deaths in 2012 of about 0.5 mln and 0.3 mln, respectively [123], see Fig. 1.2. The most difficult-to-treat cancers give a poor survival prognosis even in case of early detection, e.g. in case of lung cancer the overall estimated 5-years survival in United States is only 18% [105]. Statistics in United States are even worse for pancreatic cancer, predicting that only about 7 out of 100 diagnosed patients will survive next 5-years [105].

That is why, almost every developed country conducts cancer research at some level, with the estimated worldwide budget of about 14,300 million euros in 2004/2005 [39]. In the war with cancer there are three predominant paths pursued by the researchers: prevention, early detection, and treatment. First one

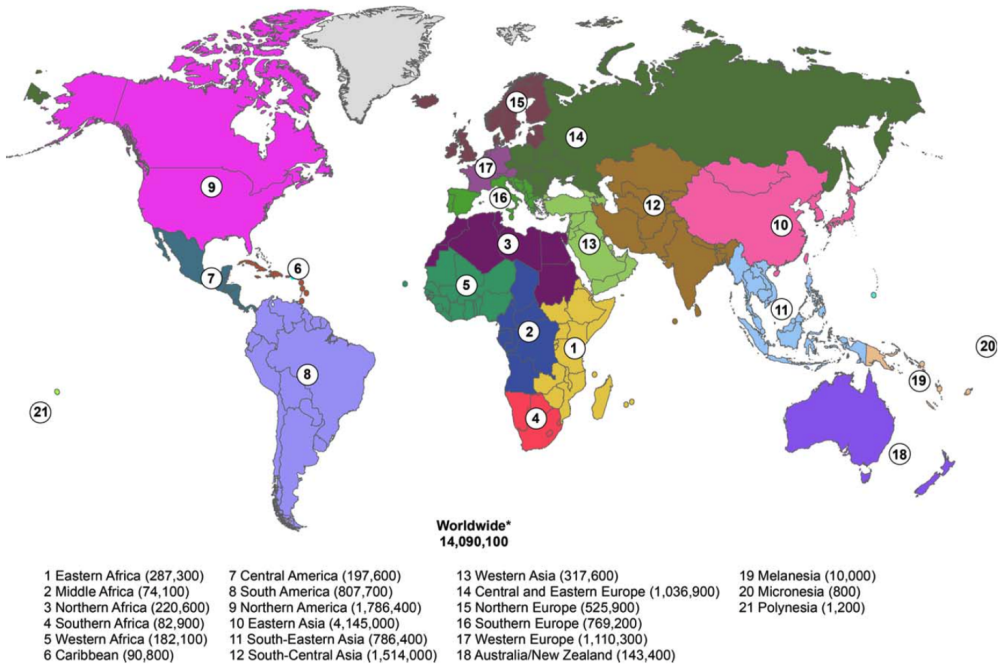

Figure 1.1: Estimated number of new cases in 2012 by the world region. Figure reproduced from [123].

attempts to reduce the death toll of cancer, by reducing its incidence rate, mostly by investigating environmental factors that increase the chance of developing cancer. The most known example of prevention program is the smoking awareness policy, that resulted in modest reduction of smoking prevalence in United States between 2005 and 2010 by 19.3% [108]. Some agencies estimate that introducing additional smoke-free legislations in United States could result in about 600,000 fewer deaths, saving more than 1 billion dollars in treatment costs [108]. The second research path focuses on developing new technologies allowing for detection of cancer on its early stages, when patient has the best prognosis and there are the best chances for complete cure. Because of the advancement in screening techniques, incidence of prostate cancers that have already spread to neighboring lymph nodes reduced in United States from about 40% to <10% in the last 50 years [110]. It is significant improvement in reducing the cancer death toll, as about 97% of prostate cancer patients will survive 10 years since the diagnosis if there is no lymph node involvement, compared to 83% otherwise [20].

The most intense research, however, is focused on developing new treatment strategies. It is estimated that the about 61% and 50% of the total cancer research budget in years 2002/03 in Europe and United States, respectively, was spent

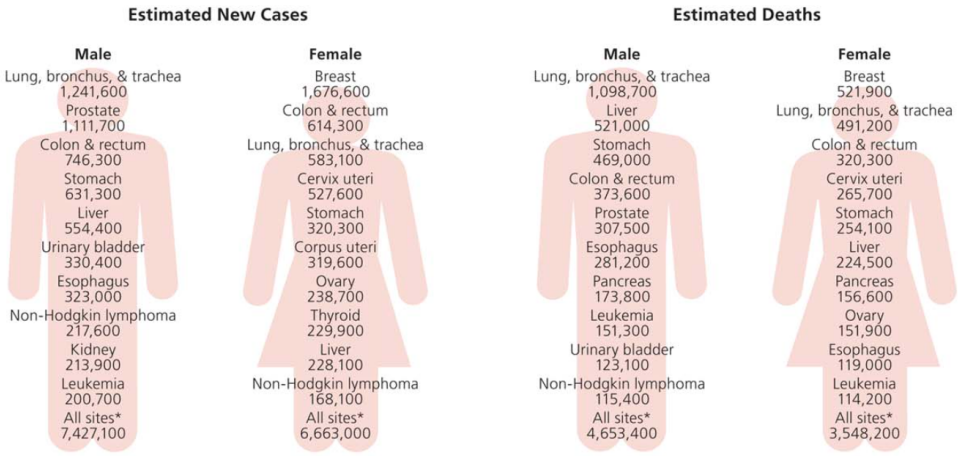

Figure 1.2: Estimated number of new cases and deaths in 2012 by type of cancer. Figure reproduced from [123].

for research focused on cancer biology and developing new treatments [39]. In recent years there were many significant breakthroughs in the treatment of particular cancers. One of the examples is approval of imatinib in the treatment of chronic myeloid leukemia, which transformed this leukemia with previous life expectancy of 4-6 years to chronic illness [107]. This makes imatinib one of the best examples of successful targeted therapy, i.e. therapy that targets molecules associated directly with cancer cells. A particularly exciting development, hailed by the editors of Science as the breakthrough of 2013 [27], is that immune surveillance might be tipped back in favor of primary and metastatic tumor regression through novel immunotherapeutic strategies. Newly developed PD-1/PDL-1 antibodies that aim to increase the efficacy of cytotoxic T lymphocytes in fighting the cancer cells have been hailed as drug of the year, as their administration results in high quality responses in metastatic melanoma patients [96]. Another example of alternative approaches to cancer treatment that was developed in last few decades is the anti-angiogenic treatment, which is designed to inhibit the tumor vascular support and thus induce tumor cell starvation [43, 44]. That kind of approach holds the promise of being less patient-specific as the host vasculature is targeted and not the constantly evolving tumor population.

However, despite those significant breakthroughs and development of alternative approaches, still in most of the cases cancer treatment consists of various combination of chemotherapy, radiotherapy and surgery. It is estimated that about 50% of all cancer patients received radiotherapy as part of their treat-

ment [30, 41] and it was administered in 40% of cases in which the primary tumor was successfully eradicated [47]. Since 1896, when the first cancer patients were treated with radiation, the main focus in development of radiotherapy has always been to design techniques allowing to deliver 100% of prescribed radiation dose to the tumor site with sparing the normal tissue at the same time [119]. The true revolution in radiotherapy started at the end of 20th century together with the development of computer-assisted treatment planning and delivery techniques [119], which allowed to significantly reduce the dose of radiation delivered to normal tissue and escalate the dose administered to tumor site. In the prostate cancer treatment the delivered dose to gross tumor volume increased 2.5-fold since 1935 [119]. Despite those significant improvements, however, there are still problems in radiobiology that remains partially unanswered and new unexpected phenomena are still being discovered. While traditional methods for measuring cellular response to radiation have included cell death and loss of colony formation, more recent findings suggest radiation induced cellular senescence may play a larger role in how a tumor responds [103]. Most interesting is the ability of senescent cells to induce angiogenesis [25] and affect neighboring cells [90]. For decades it was thought that the radiation induces changes only in tissues within the irradiated volume. However, experiments revealed that there are changes induced outside the radiation field that may influence the treatment outcome, so called bystander effects [7]. It has been also shown that radiation triggers a specific type of cell death that makes cancer cells more “visible” to the immune system and thus, potentially triggers the secondary wave of immune response [124]. Taking into account how frequently radiotherapy is used worldwide in the war against cancer, it is of the utmost importance to decipher these processes, incorporate findings in clinical practice and potentially increase treatment efficacy.

Overwhelming complexity of processes that occur in response to cancer therapy is now frequently deciphered using mathematical models, by the researchers working in a relatively new field termed mathematical oncology. It is a powerful approach in which, experimental and clinical data are utilized to build and calibrate quantitative models. There are many examples of successful application of mathematical modeling in treatment design. We need to mention a model for erythroid production based on a continuous maturation-proliferation scheme developed by Lasota and colleagues [65]. Its analysis showed how to cure specific types of therapy induced anemia. There are also several examples of successful application of mathematical models for the cancer treatment analysis. A mathematical model of cytotoxic T lymphocyte (CTL) immunotherapy predicted that cellular adoptive immunotherapy may have previously failed in glioblastoma

(GBM) patients as the administered dose is up to twenty times lower than would be required for tumor eradication in the brain, which is protected by the blood-brain barrier [62]. Model simulations suggested that dose-intensive strategies are essential, and simulation-supported recommendations of therapy dose and duration may allow personalization of CTL therapy in GBM. A recent study that iteratively combined experimental and mathematical modeling revealed optimized radiotherapy protocols for platelet-derived growth factor-driven glioblastoma [67]. Using a simple mathematical model informed with experimental data of *in vivo* dose-dependent radiation response, the authors simulated response to the conventional 2 Gy per day radiation fractionation protocol and compared it to hypo- and hyperfractionation regimens as well as arbitrary dose schedules with identical total dose. The mathematical model predicted that doses delivered at varying frequencies could provide similar tumor regression as standard of care fractionation but prolonged growth delays – results that were subsequently verified in animal studies. The study exemplifies that an integrated multidisciplinary approach can provide the urgently needed scientific methodology to design optimized therapies.

1.2 Hypothesis and specific aims

The thesis aims at improving the understanding how tumor and surrounding tissue respond to radiotherapy, through combining mathematical modeling with experiments. We hypothesize that radiation, through inducing cellular senescence in both cancer and normal cells, can trigger tumor angiogenesis and boost the growth of previously dormant tumors in the neighborhood of primary site. This effect, however, depends on the TP53 gene status as it controls the cell fate based on the amount of DNA damage induced by radiation. Thus, we postulate that, depending on the TP53 gene status, radiation combined with anti-agniogenic treatment in the form of adjuvant therapy can improve cancer treatment outcome in the case of localized diseases.

In order to verify the postulated hypothesis, this thesis will be organized around the following specific aims.

Specific Aim 1 Determine experimentally if and to what extent radiation induces cellular senescence (directly or through bystander signals) in cancer and normal cell lines.

- **Aim 1A**: Irradiate human colorectal cancer cells and co-incubate them with non-irradiated cells of the same type. Perform experiments for cells that differ by TP53 gene status. Quantify amount of induced senescence.

- **Aim 1B**: Irradiate normal human fibroblasts and co-incubate them with non-irradiated cells of the same type. Measure amount of induced senescence.

Specific Aim 2 Design and analyze mathematical model of tumor growth under angiogenic signaling.

- **Aim 2A**: Derive the mathematical model of tumor growth under angiogenic signaling, which incorporates the pathology of newly developed tumor vasculature. Extend the model by incorporating the influence of anti-VEGF focused treatment approaches.

- **Aim 2B**: Analyze the proposed model and simulate different scenarios.

Specific Aim 3 On the basis of proposed model investigate efficacy of different treatment approaches for tumor that grows under angiogenic signaling.

- **Aim 3A**: On the basis of proposed model state and analyze the optimal control problem (optimal treatment schedule and dosage problem) for the anti-VEGF tumor treatment. Utilize the Pontryagin Minimum Principle and analyze the possible solutions to the adjoint problem. Design and implement efficient procedures to solve the problem numerically.

- **Aim 3B**: Perform both local and global sensitivity analysis of proposed model. Implement Fourier Amplitude Sensitivity Test method and perform variance decomposition on different stages of tumor growth (at different time points). Investigate different possible scenarios for therapeutic intervention.

1.3 Outline for the dissertation

Chapter 1: Introduction. This introduction.
Chapter 2: Background and hypothesis. Provides details about the biological processes considered in the performed experiments and mathematical models. In Chapter 2 we also clearly state hypothesis stated and investigated in this dissertation.
Chapter 3: Experimental results. Describes materials and methods used in experiments together with summary of obtained results.
Chapter 4: Tumor angiogenesis model. In this chapter we derive in detail the model of tumor growth under angiogenic signaling. We perform its analysis and

show simulations of different possible scenarios. In Chapter 5 we also fit the model to the experimental results available in the literature.
Chapter 5: Optimal control. Describes considered optimal control problem for anti-VEGF treatment and provides its solution for certain cases. In Chapter 6 we also show few possible numerical solutions to the optimal control problem.
Chapter 6: Sensitivity analysis. Describes the results of both local and global sensitivity analyses performed for the proposed model. We focus on effectiveness of different treatment approaches on different stages of tumor growth.
Chapter 7: Summary.

1.4 List of publications

Results presented in the dissertations were published in the following peer-reviewed articles:

1. **Poleszczuk J.**, Hahnfeldt P., Enderling H. Therapeutic implications from sensitivity analysis of tumor angiogenesis models. PloS ONE 2015;10(3): e0120007.

    - **Citations**: 0
    - **5 Year IF (2014)**: 3.702
    - **Contribution**: I came with idea for the study while visiting P. Hahnfeldt and H. Enderling in the Center of Cancer Systems Biology in Boston at the beginning of 2012. I've performed data fitting of the models to the experimental data from murine models, as well as local and global sensitivity analysis. Percentage contribution: 90%.

2. **Poleszczuk J.**, Piotrowska M.J., Foryś U. Optimal protocols for the anti-VEGF tumor treatment. Mathematical Modelling of Natural Phenomena 2014;9(4): 204–15.

    - **Citations**: 1
    - **5 Year IF (2014)**: 0.807
    - **Contribution**: 90%. I came with idea for the study during XVIIth National Conference on Application of Mathematics to Biology and Medicine, where I was presenting the results of my previous research on anti-angiogenic treatment modeling. I've formulated and analyzed the optimal control problem discussed in the paper. Percentage contribution: 90%.

3. **Poleszczuk J.**, Bodnar M., Foryś U. New approach to modeling of antiangiogenic treatment on the basis of Hahnfeldt et al. model. Mathematical Biosciences and Engineering 2011;8(2): 591–603.

    - **Citations**: 10
    - **5 Year IF (2014)**: 1.128
    - **Contribution**: The research contained in the article is an extension of my work done during MSc studies. I've derived the model considered in the paper, and worked together with M. Bodnar and U. Foryś on its mathematical analysis and numerical simulations. Percentage contribution: 50%.

Other studies performed during PhD studies that are directly related to the topics considered in this dissertation were published in the following peer-reviewed articles:

1. **Poleszczuk J.**, Krzywon A., Forys U., Widel M. Connecting radiation-induced bystander effects and senescence to improve radiation response prediction. Radiation Research 2015;183(5): 571–577.

    - **Citations**: 0
    - **5 Year IF (2014)**: 2.880
    - **Contribution**: I came with idea for the study when I first visited the group of my thesis co-supervisor, Prof. Maria Wideł. I helped with the experimental design of the study, proposed mathematical model of senescence associated bystander signaling, and performed its data fitting to the experimental data. Percentage contribution: 70%.

2. Widel M., Lalik A., Krzywon A., **Poleszczuk J.**, Fujarewicz K., Rzeszowska-Wolny J. The different radiation response and radiation-induced bystander effects in colorectal carcinoma cells differing in p53 status. Mutation Research 2015;778: 61–70.

    - **Citations**: 0
    - **5 Year IF (2014)**: 3.521
    - **Contribution**: The work is an extension to the work published in [90]. I've helped with the design of the study. Percentage contribution: 10%.

3. **Poleszczuk J.**, Hahnfeldt P., Enderling H. Biphasic modulation of cancer stem cell-driven solid tumour dynamics in response to reactivated replicative senescence. Cell Proliferation 2014;47(3): 267–276.

    - **Citations**: 2
    - **5 Year IF (2014)**: 2.777
    - **Contribution**: The idea for the study was proposed by H. Enderling while I was visiting the Center of Cancer Systems Biology in Boston at the beginning of 2012. I've implemented his idea in the form of cellular automaton model, performed all simulations and subsequent analysis of the results. Percentage contribution: 70%.

4. Piotrowska M.J., Bodnar M., **Poleszczuk J.**, Foryś U. Mathematical modelling of immune reaction against gliomas: Sensitivity analysis and influence of delays. Nonlinear Analysis: Real World Applications 2013;14(3): 1601–1620.

    - **Citations**: 2
    - **5 Year IF (2014)**: 2.322
    - **Contribution**: In this study I performed the global sensitivity analysis for the considered mathematical model. I've implement the Fourier Amplitude Sensitivity Test and subsequently proposed how to simplify the model. Percentage contribution: 25%.

Chapter 2

Background and hypothesis

This Chapter describes the biological processes and mechanism that are an integral part of the investigated hypothesis. It begins with description of changes induced in a cell after exposure to ionizing radiation, and existing cellular mechanisms to counteract them. It provides description of the basic functions of p53 protein, which is one of the most important proteins involved in cellular response to DNA damage caused by radiation. After direct exposure to radiation, depending on the status of the TP53 gene (gene that encodes p53 protein), cell can either die or acquire several distinct phenotypes. A particularly interesting phenotype is senescence, which is described in the subsequent section. After considering radiation response on a single cell level, the chapter focuses in two subsequent sections on the response to radiation on a population level. First, it introduces the concept of radiation-induced bystander effects that have been intensively studied by experimentalists for the last few decades. Then, it describes the process of tumor angiognesis, which for decades has been considered as a promising target for cancer therapy. The chapter ends with detailed statement of the hypothesis, which is investigated in the thesis.

2.1 Influence of ionizing radiation on a cell

Ionizing radiation, which is frequently utilized in cancer therapy, gives a charge to the atoms that were previously electrically neutral by removing tightly bound electrons from their orbits [106]. Ionization of nucleobases (cytosine, guanine, adenine, and thymine), the basic building blocks of DNA, can result in breaks of DNA strands and thus, can introduce errors in genetic material whose integrity is essential for cell function and survival [2]. However, most of the DNA breaks

that occur after exposure to the ionizing radiation are caused not by the direct ionization of nucleobases, but by the interaction of DNA strands with radiation-induced water-derived radicals [59, 98], see Fig. 2.1.

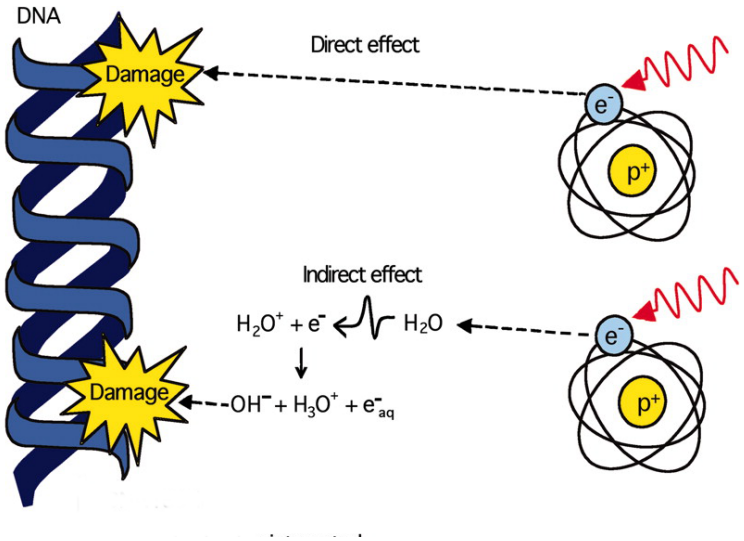

Figure 2.1: Breaks in the DNA strands can occur directly through ionization of DNA molecules or indirectly through interactions of DNA with radiation-induced water-derived radicals. Figure reproduced from [79].

Breaks in the DNA are being detected by a specialized proteins, which then initiate a various signaling cascades through mediator proteins. This results in many changes on a cellular level, such as initiation of the DNA repair mechanisms, arrest of the cell cycle at the regulation point in order to extend the time available for necessary repairs, increase in the availability of DNA building elements (deoxynucleotides, dNTPs), or, if the damages are to extensive, initiation of the programmed cell death process termed apoptosis [56], see Fig. 2.1. Single strand breaks are relatively easy to repair by the available cellular mechanisms, as the second intact strand carries information about proper structure of the genetic material. Not always properly repaired and thus, potentially harmful for a cell, are so-called double strand breaks (DSBs), i.e. breaks on both DNA strands occurring so close to each other that the DNA splits into two parts [56, 64].

The p53 protein is one of the most important proteins regulating the response of a cell to DNA damage. Its main function, in case of damage detection, is to arrest the cell cycle in G_1 phase in which cell prepares enzymes necessary for the DNA replication in subsequent phases [38]. Elongating G_1 phase duration gives the cell time to repair the DNA and thus, decreases the chance of passing faulty genetic material to daughter cells. Moreover, if the damages are too extensive

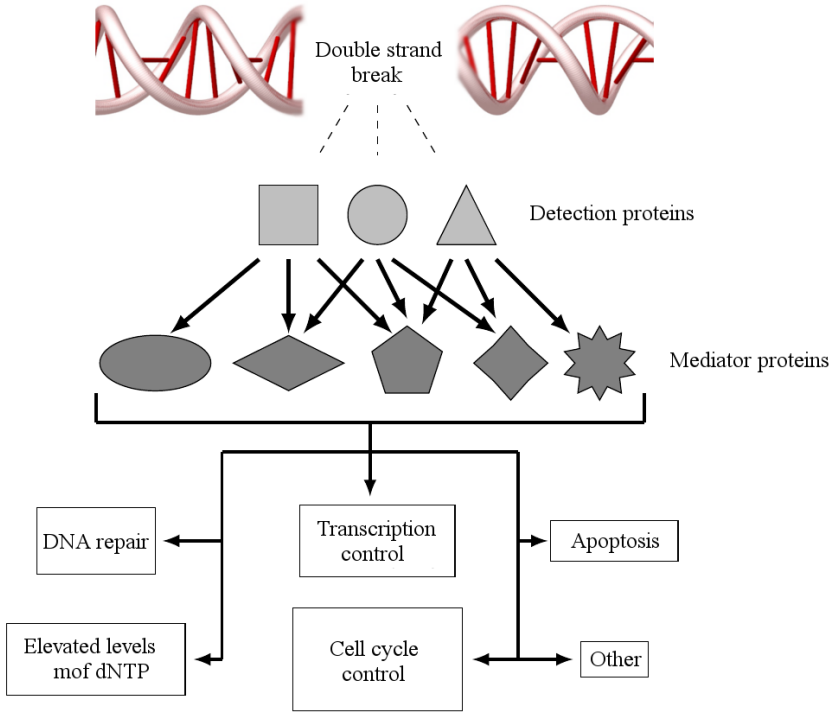

Figure 2.2: Schematic representation of the cell response to double strand break (DSB). Detection proteins sense a new newly created DSB and send a downstream signal to mediator proteins, which in turn affect multiple signaling pathways.

or the repair fails, p53 protein can trigger the programmed cell death pathway – apoptosis [46, 78]. The TP53 gene, which encodes the p53 protein, is frequently called the "guardian of the genome", because of such an important role in keeping consistency of genetic information stored in the DNA. Interestingly, mutations of TP53 gene that impair the functioning of p53 protein are common feature among human cancers [49]. In case of the lung, colon and ovarian cancer, mutation of TP53 gene is found in about 50% of all diagnosed cases [49].

2.2 Cellular senescence

In 1961, Hayflick and Moorhead reported that extensively cultured human primary cells cease to proliferate after a finite number of divisions [54] yet remain viable and metabolically active [17, 61]. Experiments with transfected telomerase, an enzyme that rebuilds telomeric DNA [50], revealed that proliferation exhaustion is a consequence of telomere erosion [6, 103]. This irreversible cy-

tostasis of the cell is termed replicative senescence. Several other factors can lead to different forms of irreversible mitotic arrest, such as DNA damage and oxidative stress (SIS - stress induced senescence; [61]), oncogenic activation (OIS – oncogene-induced senescence; [104]), or loss of tumour suppressor genes (PICS - PTEN loss-induced cellular senescence; [19]). Senescent cells display altered cell morphologies, overexpress plasminogen activator protein 1 (PAI-I), and present β-galactosidase [16, 97], see Fig. 2.3. Experiments suggest that cells with functional p53 appear more sensitive to stress and oncogene activities that stimulate senescence [5]. Initially, cellular senescence was believed to be a side

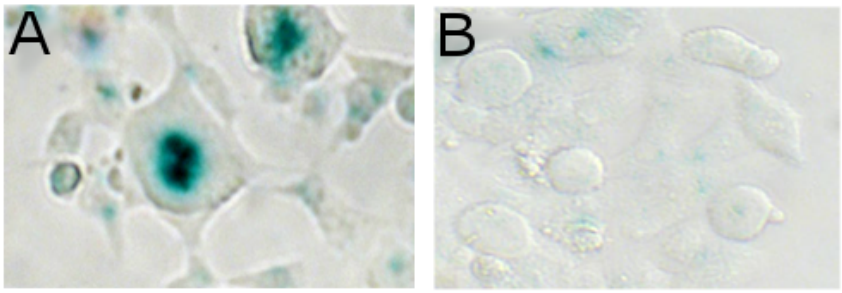

Figure 2.3: Human colorectal cancer cells in senescent state (A) and undergoing apoptosis (B) after exposure to 8 Gy of radiation. Senescent cells display characteristic enlarged morphology and over-expression of β-galactosidase (stained in green). Pictures from own experiments.

effect of culturing cells *in vitro*, but recently senescent cells have also been detected *in vivo* in a variety of tissues in a number of different organs [22]. The senescence program is believed to protect tissue integrity by disabling mitosis in stressed or damaged cells – therefore likely acting as a tumour suppressor [73]. During carcinogenesis, cells acquire traits that enable circumvention of replicative senescence – a hallmark of cancer [52, 53, 71]. It has been suggested, however, that the cellular senescence pathways remain intact in tumours [101] and can be reactivated through cell autonomous programs [126]. What is most important, it has been reported that cellular senescence can also be triggered, and might actually be the predominant response to ionizing radiation and many currently used chemotherapeutic drugs [61, 71, 83]. Growth arrest in these cases is achieved and maintained, in part, by the increased expression of specific cyclin-dependent kinase inhibitors, including p16Ink4a [42].

Recent studies have shown that senescent cells can exert harmful effects on the tissue microenvironmnet, mainly by the acquisition of a senescence-associated secretory phenotype (SASP) [29]. Further, SASP seems to be conserved across

cell types and species and it has been shown that it is triggered after a treatment of cancer patients with DNA damaging chemotherapy [26]. SASP is accompanied by a huge increase in the secretion of over 40 intercellular signaling factors, which may have various effects on the surrounding cells [24, 129], such us promotion of the proliferation and tumorigenesis of epithelial cells [63]. Senescent cells have been also shown to release nitric oxide and ROS [127], which are one of the intercellular signaling molecules that elicit the radiation induced bystander effect [99]. What is most important, it has been shown that human fibroblast in the senescent state secrete vascular endothelial growth factor [25] and thus, can trigger the angiogenesis process.

2.3 Radiation-induced bystander effects

Radiation induced bystander effects (RIBE) are defined as the induction of biological changes in cells that are not directly exposed to ionizing radiation, but are only subject to signals released by their irradiated neighbors, see Fig. 2.4. For the last two decades they have attracted significant attention due to their possible implications for radiotherapy; see [99] and references therein. Classical RIBE include negative influence of signals released by the irradiated cells on unirradiated cells, such as: reduced clonogenic survival [81], increased sister chromatid exchange [70], formation of micronuclei and apoptosis [95]. Other types of RIBE include effects such as: increased survival of non-targeted cells when the targeted cells received a high dose of radiation [99]; an increase in the survival of cells targeted by a high radiation dose when neighboring cells received a low radiation dose [74]. Various cell types present variable radiosensitivity and bystander response, which can depend on, among others, the genetic status, the experimental setting and endpoint investigated [7]. One of the most intensively studied genes in RIBE research is the TP53 tumor suppressor gene, which is involved (through its own product - the p53 protein) in DNA repair, cell cycle regulation and apoptosis [21, 75, 121]. The role of the TP53 gene in RIBE is, however, inconclusive. The appearance of DNA double-strand breaks accompanied by binding of the protein 53BP1 (p53-binding protein 1), has been detected as 53BP1 foci not only in the nuclei of cells irradiated by individual alpha particles, but also in the adjacent non-irradiated cells [118]. Similarly, p53 protein expression was observed in the rat lung epithelial cells adjoining the cells targeted with alpha particles [55]. On the other hand, it has been shown that both HCT116 cells with p53-wild type and p53-knockout gene induced bystander effect appearing as decrease of clonogenic cell survival [80]. This indicates the en-

gagement of p53 pathway in response to bystander signals, though cells lacking a functional p53 may still generate such signals. Other experiments performed on normal human fibroblasts [122] revealed that cells with wild type p53 were not only restrained in releasing the bystander signals after irradiation, but were also resistant to the signals released by the mutated p53 cells. Although the identity of the molecular pathways associated with RIBEs has not been completely elucidated, several intercellular and intracellular signaling molecules implicated in bystander signaling have been identified; see [99] and references therein, notably including ROS, nitric oxide, Interleukin 8 and NF-κB protein.

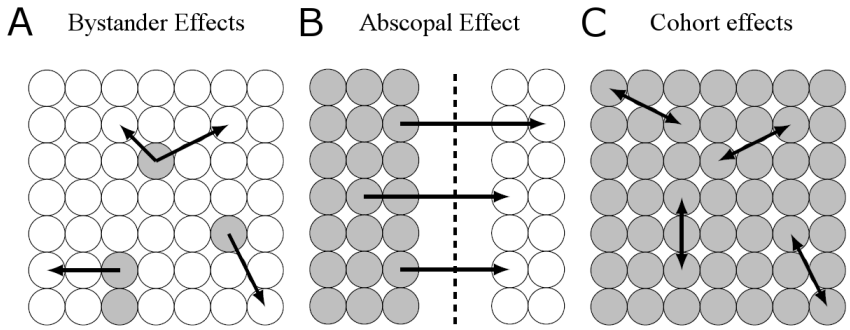

Figure 2.4: Different (non-mutually exclusive) scenarios of multi-cellular responses to radiation. In bystander (A) effects irradiated cells (gray circles) communicate with non-irradiated cells (white circles) within the irradiation field. In abscopal responses (B) non-irradiated cells outside the radiation volume are affected. In cohort effects (C) we consider signaling between irradiated cells.

2.4 Tumor angiogenesis

In 1971 Judah Folman in [43] wrote that growth of any tumor is strongly dependent on the amount of blood vessels that it induces to grow. He surmised that, if a tumor could be stopped from growing its own blood supply, it would wither and die. In adults normal physiological role of angiogenesis – the process of new vessels formation – is restricted to wound healing, the menstrual cycle and pregnancy. In addition, angiogenesis is critical during fetal development. Unfortunately, it is also essential for the successful growth and development of solid tumors. After reaching avascular dormant state tumor can grow further only by inducing vessels in host tissue to sprout capillary tubes which migrate towards and ultimately penetrate the tumor, providing it with a circulating blood supply and, therefore, an additional source of nutrients [57, 58].

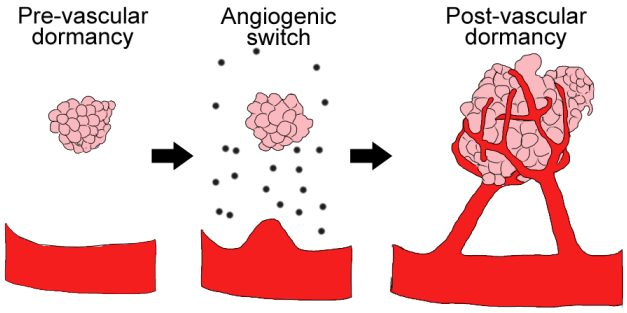

Figure 2.5: Schematic representation of tumor angiogenesis process. After reaching avascular dormant state, tumor can grow further only by inducing vessels in the host tissue to sprout capillary tubes which migrate towards and ultimately penetrate the tumor, providing it with a circulating blood supply, and therefore an additional source of nutrients.

Despite the essential role of angiogenesis in tumor growth, it has been discovered that tumor angiogenesis is highly pathological. Incorrect structure and poor efficiency of newly formed vessels are common tumor features [57, 58]. Some trials which where developed to investigate tumor biology revealed that most of administrated dose of chemotherapy is not even absorbed by tumor. Moreover, absorbed part of dose was not distributed evenly in particular tumor regions. It makes effective tumor treatment difficult, because cells which do not get sufficient amount of drug can survive and even if they are only few repeated tumor growth is inevitable.

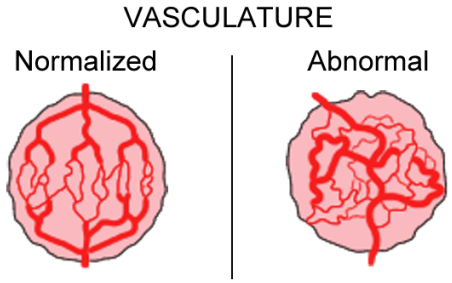

Figure 2.6: Pathology of tumor angiogenesis. Abnormal structure (right) and poor efficiency of newly formed vessels are common tumor features. Anti-angiogenic drugs improve chemotherapy by causing “vessel normalization” in tumors (left).

2.5 Working hypothesis

In the preceding sections we have reported existing experimental evidence that the senescence can be induced directly by the ionizing radiation, with the magnitude depending on the TP53 gene status. We discussed the influence of senescent cells on the surrounding tissue, providing reports showing that senescent cells can trigger the angiogenesis process. We have also reported the current knowledge about bystander effects, phenomena in which cells non-exposed to radiation are affected by the signals from irradiated cells.

We hypothesize that senescence can be also induced in the cells residing outside of the irradiated volume through bystander signaling. To verify that statement we perform series of experiments on both cancer and normal human cell lines in which we co-incubate irradiated cells with non-irradiated ones (Specific Aim 1). It is conceivable that in the *in vivo* setting senescent cells induced outside of the irradiation field can trigger the angiogenesis process and thus, boost the growth of micro-tumors residing outside of the irradiation field. It is worth to mention that in case of the breast cancer studies have shown that subclinical disease occurs in 52% and 25% of the specimens at distances >10mm and >20mm, respectively, from the gross tumor volume captured at MRI images [102]. Thus, we hypothesize that the radiotherapy combined with the anti-angiogenic drug could improve the treatment outcome. This, unfortunately, can be verified only in clinical trials or murine models, which are outside of the scope of this thesis. However, even before attempting to design a clinical trial or murine experiment, one needs to know the dosage at which the anti-angiogenic drug should be applied. That is why, in Specific Aim 2 we develop and analyze a mathematical model of tumor growth under angiogenic signaling that incorporates the effect of anti-angiogenic drugs and in subsequent Specific Aim 3, we state an optimal control problem for anti-angiogenic treatment to derive the best clinical protocols. In Specific Aim 3 we also investigate other treatment approaches using tools of sensitivity analysis.

Chapter 3

Experimental results

This Chapter presents experiments performed to verify if cellular senescence can be induced through radiation-induced bystander signaling. These experiments were planned and performed with the group of Prof. Maria Wideł, who is co-supervisor of this dissertation. The Chapter starts with the detailed description of materials and methods used in the experiments. Briefly, irradiated (2, 4, 6 and 8 Gy) human colorectal carcinoma cells (HCT116) with wild (p53 +/+) or knockout (p53 −/−) TP53 gene were co-incubated with non-irradiated cells of the same type. Senescence assays were used for both irradiated (IR) and only co-incubated (By) populations. In order to asses the radiation response in normal tissue, the same set of experiments was performed for normal human dermal fibroblasts (NHDFs). In subsequent sections of the Chapter we report experimental results. Briefly, we observed that senescence is effectively induced in bystander populations for both HCT116 p53 +/+ and NHDF cell lines, with the magnitude depending on the radiation dose. We didn't observe significant changes in the fraction of senescent cells in bystander populations for HCT116 p53 −/− cells. However, additional experiments performed only for NHDFs make us believe that in the case of HCT116 p53 −/− cell line senescence induction was not detected as a result of too short co-incubation period.

3.1 Materials and Methods

Human colorectal carcinoma HCT116 wild type (p53 +/+), p53 null (p53 −/−) and NHDF cell lines were obtained from the Culture Bank of Center of Oncology-Gliwice. The HCT116 p53 +/+ line was originally purchased from American

Type Culture Collection; HCT116 p53 −/− was kindly donated by Prof. Bert Vogelstein (The Ludwig Center at Johns Hopkins University, Baltimore, USA).

3.1.1 Culture system and irradiation

All cell lines were routinely tested for mycoplasma and cultured at 37 °C in a humidified CO2 incubator in Dulbecco's modified Eagle's medium/F12 Ham (1:1) (Sigma-Aldrich) supplemented with 12% heat-inactivated fetal bovine serum (FBS; PAA, Immuniq, Poland) and 80 μg/ml gentamicin (Krka, Poland). Cells to be irradiated were seeded 20 hours before the experiment (1.0×10^5 cells/well in 3 ml medium) into 6-well dishes (BD Immunogen, see Fig. 3.1) and incubated.

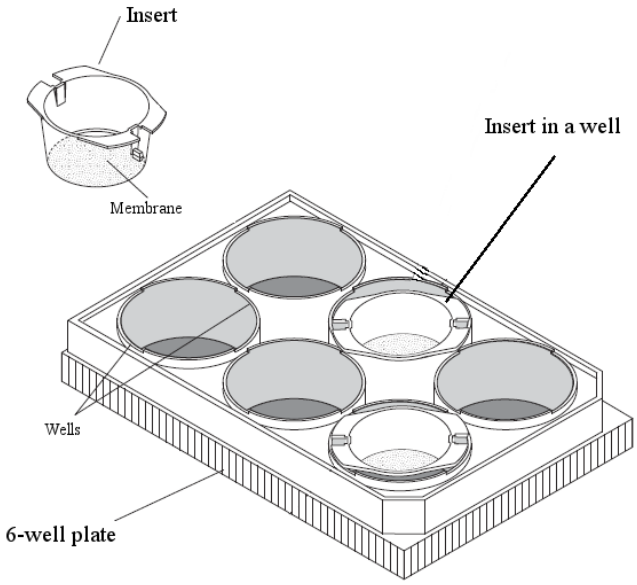

Figure 3.1: Cell culture plate used in bystander experiments. Non-irradiated cells in inserts are inserted into one of 6 wells containing cells exposed to ionizing radiation.

Simultaneously, the same number of cells was seeded on inserts with membrane bottom of 0.4 μm pore size (BD Immunogen), inserted into sterile 6-well dishes, and incubated. Confluence of cells before irradiation was about 50%. Cells in 6-well dishes were irradiated at a room temperature with 2, 4, 6, 8 Gy single doses of X-rays (6 MV) generated by the therapeutic accelerator Clinac 600. Immediately after irradiation, inserts with non-exposed cells were inserted into wells and co-incubated for a range of periods. The schematic representation of the experimental procedure is shown in Fig. 3.2.

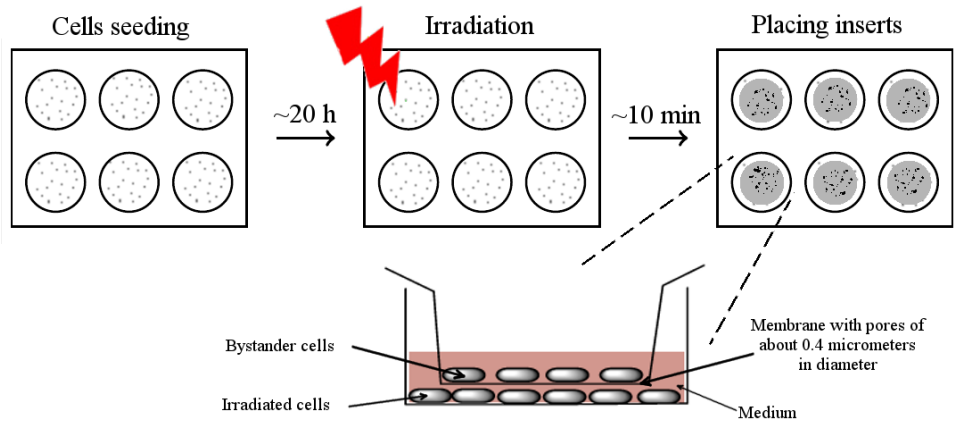

Figure 3.2: Experimental setting used in bystander experiments. Both cells to be irradiated and bystanders were seeded about 20 h before irradiation. About 10 minutes after irradiation inserts were inserted into wells.

3.1.2 Senescence assay

After co-incubation period, senescent cells were evaluated in situ directly in the wells and inserts using a widely used and accepted biochemical marker, senescence-associated β-galactosidase (SA-β-gal) activity [109]. It has been shown in [32] that expression of SA-β-gal distinguishes senescent cells from proliferating and quiescent ones. For the SA-β-gal staining we used Senescence Cells Histochemical Staining Kit (Sigma-Aldrich) in accordance to the original protocol. Staining was evaluated after ~16 h incubation at 37 °C in a CO2-free incubator. The percentages of β-galactosidase positive cells were determined using inverted microscope by scoring at least 1000 cells/sample (one of the acquires images is shown in Fig. 3.3). Characteristic flattened and enlarged morphology

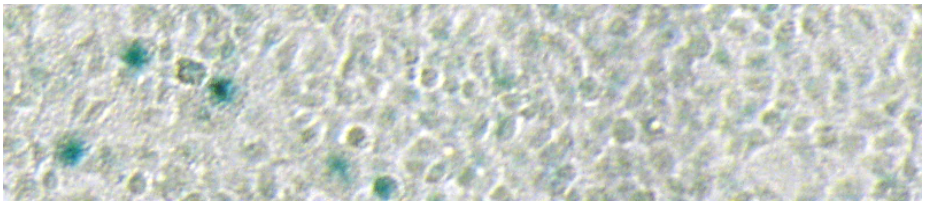

Figure 3.3: Exemplary image fragment of the culture plate stained for senescence-associated β-galactosidase (SA-β-gal).

of the senescent cells, with a prominent nucleus and increased cytoplasmic granulation, was also taken into account. Presented results are the averages from 4 independent experimental sets.

3.2 Results

3.2.1 Senescence induction in bystander populations

In the first set of experiments we quantified amount of induced senescence in both irradiated and bystander populations after 48 h of co-incubation. We found that p53 positive HCT116 cells are much more vulnerable to radiation induced senescence than their p53 negative counterparts, compare Fig. 3.4. We observed

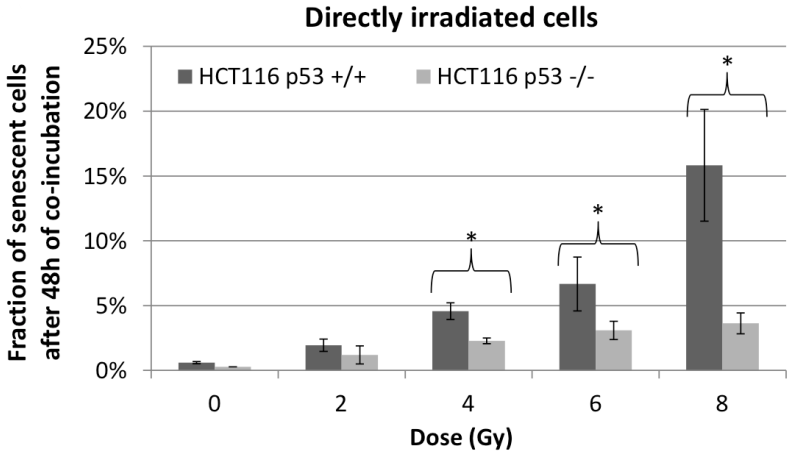

Figure 3.4: Fraction of senescent cells in p53 $+/+$ and p53 $-/-$ colorectal carcinoma cell lines (HCT116) exposed to direct radiation. Asterisk denotes statistically significant difference (p-value<0.05; Student's t-test). Presented data are the means ± SD.

that the higher the radiation dose, the larger the difference between the cell lines in the fraction of senescent cells (4.57% vs. 2.28% at 4 Gy and 15.81% vs. 3.63% at 8 Gy for directly irradiated p53 $+/+$ and p53 $-/-$ cell lines, respectively). The same qualitative behavior was found in the bystander populations, compare Fig. 3.5. For p53 positive bystander population we obtained a 6-fold increase in the fraction of senescent cells compared to the untreated control.

Similar response to radiation was observed for NHDF cell line, compare Fig. 3.6. After direct exposure to 6 Gy of radiation about 14% of NHDF population acquired senescent phenotype, which is a significant increase compared to almost negligible fraction of senescent cells in the untreated control (p-value<0.05; Student's t-test). We observed the same qualitative behavior in the bystander population, for which about 8% of cells acquired senescent phenotype after co-incubation with population irradiated using 8Gy of radiation.

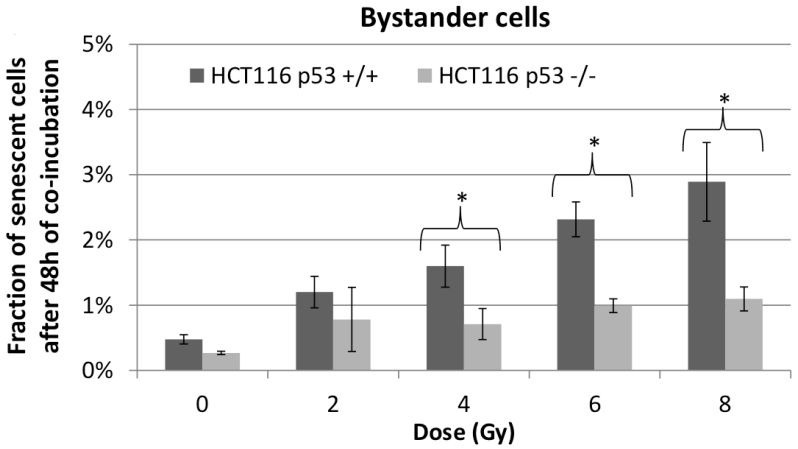

Figure 3.5: Fraction of senescent cells in p53 +/+ and p53 −/− colorectal carcinoma cell lines (HCT116) co-incubated with the cell exposed to direct radiation. Asterisk denotes statistically significant difference (p-value<0.05; Student's t-test). Presented data are the means ± SD.

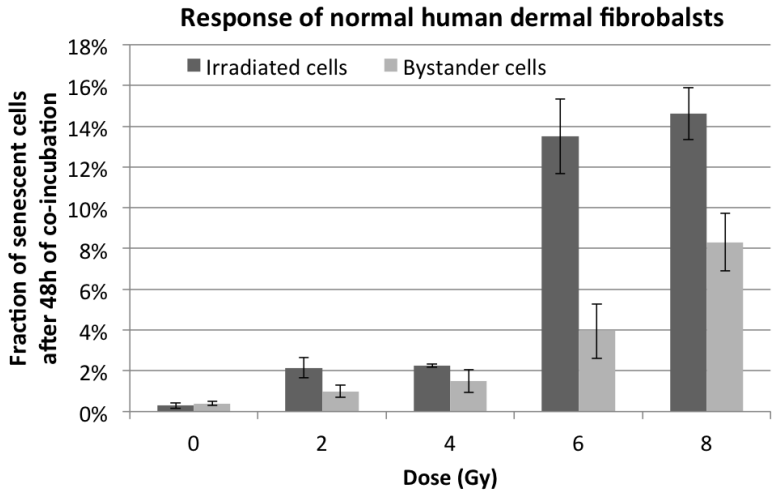

Figure 3.6: Fraction of senescent cells in normal human dermal fibroblasts cell line (NHDF) exposed to direct radiation and co-incubated with irradiated cells. Presented data are the means ± SD.

3.2.2 Senescence induced senescence

In the second part of experiments we set on to answer if changes induced in the bystander populations can propagate further into the tissue, i.e. cells from inserts can induce senescence in untreated cells. We designed three experimental setups

for NHDF cell line:

- **Control**: co-incubate directly irradiated cells (0, 2 and 6 Gy) with non-irradiated bystanders for 96 hours. Quantify the amount of senescence in wells.

- **Group 1**: co-incubate directly irradiated cells (0, 2 and 6 Gy) with non-irradiated bystanders for 48 hours and then remove the inserts. Continue incubation of irradiated cells without inserts for additional 48 hours. Quantify amount of senescence in wells.

- **Group 2**: place inserts removed after 48 hours in Group 1 into wells containing untreated cells and co-incubate them for 48 hours. Quantify amount of senescence in wells.

If there is a positive feedback loop, i.e. cells acquiring changes through bystander signaling can induce senescence in untreated cells, we can expect that the fraction of senescent cells will be larger in Group 1 compared to the Control. We can expect also a significant increase in the amount of senescence in Group 2 compared to cells that were not exposed to any radiation (0 Gy from all groups).

In the experimental results, however, we did not detect any significant differences between Control and Group 1, compare Fig. 3.7. The increase in the

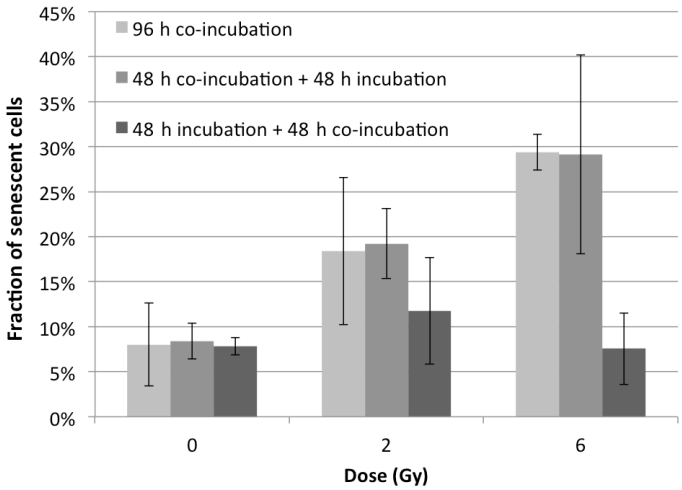

Figure 3.7: Fraction of senescent cells in normal dermal fibroblasts NHDF line from experimental control group (96 h co-incubation), group 1 (48 h co-incubation + 48 h incubation), and group 2 (48 h incubation + 48 h co-incubation). Presented data are the means ± SD.

fraction of senescent cells within the irradiated population was indistinguishable between both groups and increased from about 5% at 0 Gy to about 30% for 6 Gy. Interestingly, the amount of senescence is noticeably higher after 96 hours of co-incubation compared to 48 hours of co-incubation, compare Figs. 3.7 and 3.6. Consistently, we did not observe any significant differences between Group 2 and untreated cells – the amount of senescent cells within populations was the same.

3.3 Conclusions

Performed experiments have clearly shown that the bystander signals can induce senescent phenotype in bystander non-irradiated populations. This effect, however, is dependent on the TP53 gene status – in the considered co-incubation periods it was detected only for cells having a functioning p53 protein. Moreover, experiments designed to verify if the bystander signal can be propagated further indicate that there are no-secondary effects on the surrounding tissue when senescence is considered. However, we observed that the fraction of senescent cells is dependent on the co-incubation period, i.e. development of senescence phenotype can take more than 48 hours. Thus, it is conceivable that the secondary effects and bystander senescence induction in p53 knockout cells could be visible after prolonged periods of co-incubation. However, confirmation is needed with subsequent experiments.

Chapter 4

Tumor angiogenesis model

This Chapter introduces mathematical model of tumor response to anti-angiogenic treatment, which was developed together with the group of my supervisor Prof. Urszula Foryś. The mathematical framework is based on the well recognized model proposed by Hahnfeldt and colleagues [51], which has been an object of my research since graduate studies [85, 87, 92]. The model has been successfully compared by Hahnfeldt and co-workers to the experimental data collected from murine models designed to investigate the effects of anti-vascular treatment, i.e. treatment focused on destroying endothelial cells that are the basic building blocks of blood vessels. For that kind of treatment, on the basis of the Hahnfeldt *et al.* model, with the usage of the optimal control theory, some protocols of anti-vascular treatment and radiotherapy were proposed [40, 68, 69, 111, 115, 117]. However, the formulation of that model in our opinion is valid only for the anti-vascular treatment and thus, we propose modification of the original model such that the anti-angiogenic treatment, that is the treatment focused on blocking angiogenic signaling, is valid. Preliminary idea of presented modification was also described in my MsC thesis. However, later on we have proposed more general model exploiting new methodology in modeling of such a treatment [86].

4.1 Introduction

Growth of tumor under angiogenic signalling was successfully mathematically described by Hahnfeldt et al. in [51]. Confirmed by laboratory experiments biological validity of the Hahnfeldt et. al model makes it probably the most important model describing this aspect of tumor development. Several other studies have incorporated mathematical models for the development of tumor under an-

giogenic signalling: see [76] and references therein or [94], where also other processes connected with tumor growth are presented. A family of models based on the Hahnfeldt *et al.* model is an object of study of several groups of researchers. D'Onofrio and Gandolfi [34–36] analyzed these models from a dynamical systems point of view. Influence of time delays which are important part of any complex biological process were studied in [8, 11, 12, 45]. Świerniak, Świerniak et al. [111, 115, 117] and Ledzewicz and Schättler [68, 69] studied these models as optimal control problems with the goal of designing optimal and suboptimal antiangiogenic protocols. In the literature we can also find models built on different, than in case of the Hahnfeldt *et al.* model, assumptions (see e.g. [1, 4]) and approaches to angiogenesis (see e.g. [9]).

The model proposed by Hahnfeldt *et al.* [51] results from the theoretical concept postulating that the tumor growth is a bidirectional control process. The tumor regulates associated vascular growth or suppression, and in turn, the tumor vasculature controls the tumor growth through its usual nutritive function. The tumor volume (V) and the effective vascular support (K), which defines the environmental carrying capacity, are time-dependent variables described by coupled ordinary differential equations (ODEs). Hahnfeldt *et al.* [51] built the model on the basis of Gompertzian tumor growth, which is one of the commonly used single population growth model. This model reads

$$\dot{V}(t) = -\varepsilon V(t) \ln \frac{V(t)}{K}, \tag{4.1}$$

where:

- $V(t)$ is the population size (here we consider the population of tumor cells) at time t;
- ε is the maximal reproduction rate, meaning the rate of reproduction for the size of population near 0;
- K is the population carrying capacity, meaning the optimal population size: if $V(t) < K$, then the population size can grow, otherwise it must decrease, and in natural populations growing from the beginning in their environment only the first situation is possible.

It is obvious that for any positive initial data $V(0) > 0$ the solution $V(t)$ of Eq. (4.1) tends to K monotonically. Hahnfeldt *et al.* [51] claimed that Eq. (4.1) could be a proper description for tumor cells only in the first avascular stage of the growth. Then, with the constant effective vascular support K_{max}, the initial rapid tumor growth is followed by a slowdown as the tumor volume approaches

environmental carrying capacity K_{max}. When angiogenesis starts, the tumor carrying capacity grows, and therefore $K = K(t)$ in such a case. Moreover, Eq. (4.1) should be complemented by an equation describing the dynamics of $K(t)$.

To account reciprocal interaction of the tumor with the host vasculature the vascular support can be described by the following relation

$$\dot{K}(t) = -\mu K(t) + bS(V(t), K(t)) - dI(V(t), K(t)), \tag{4.2}$$

where $-\mu K(t)$ represents the spontaneous loss of functional vasculature, the term $bS(V(t), K(t))$ represents the stimulation of vessels growth, while $-dI(V(t), K(t))$ describes the endogenous inhibition of previously generated vasculature.

To derive the relationship between the functions $I(V, K)$ and $S(V, K)$ Hahnfeldt *et al.* considered a partial differential equation for the concentration of angiogenic stimulators/inhibitors from which the following relationship between $I(V, K)$ and $S(V, K)$ was derived

$$\frac{I(V, K)}{S(V, K)} = V^{\alpha} K^{\beta}, \quad \text{where } \alpha + \beta = 2/3,$$

see [51, 87] for further details. We shall follow this idea in the next Section, proposing our modification of this model.

Hahnfeldt *et. al* proposed to consider $\alpha = -1/3$ and $\beta = 1$, that is the stimulatory capacity and the endogenous inhibition functions given by $V(t)$ and $K(t)V^{2/3}(t)$, respectively. However, other forms of those functions were considered by other authors, compare Tab. 4.1, and hence one can consider the whole family of the tumor angiogenesis models. Introduction of other stimu-

$S(V(t), K(t))$	$I(V(t), K(t))$	Ref.
$V(t)$	$K(t)V^{2/3}(t)$	Hahnfeldt *et al.* [51]
$K^{2/3}(t)$	$K^{4/3}(t)$	Ergun *et al.* [40]
$K(t)$	$K(t)V^{2/3}(t)$	d'Onofrio and Gandolfi [34]

Table 4.1: Formulas for the stimulatory capacity function $S(V, K)$ and the endogenous inhibition function $I(V, K)$ considered in the literature.

lation/inhibition functions was motivated by the biological evidences [34] or it was dictated by easier tractability of the associated optimal control problem [40]. However, it can be shown (see e.g. [84]) that for all formulas presented in Tab. 4.1

and arbitrary positive initial conditions $V_0 > 0$ and $K_0 > 0$, the corresponding solution (V, K) of Eqs. (4.1) and (4.2) exists for all $t \geq 0$, is unique and both V and K remain positive. In addition, there are only two possible scenarios depending on the parameter values: there exists a unique positive globally asymptotically stable steady state in $\mathbb{R}^2_+$ or there is no positive steady state and the solution (V, K) tends to $(0, 0)$ as $t \to +\infty$.

The classical Hahnfeldt *et al.* model includes also additional term describing anti-vascular treatment. Therefore, the second equation of the model takes the form

$$\dot{K}(t) = -\mu K(t) + bS\left(V(t), K(t)\right) - dI(V(t), K(t)) - eK(t)u(t)\,, \tag{4.3}$$

where $u(t)$ describes the concentration of drug which is typically referred as to antiangiogenic.

Eventually, the Hahnfeldt *et al.* model reads

$$\begin{aligned} \dot{V}(t) &= -\varepsilon V(t) \ln \tfrac{V(t)}{K(t)}, \\ \dot{K}(t) &= -\mu K(t) + bV(t) - dK(t)(V(t))^{2/3} - eK(t)u(t). \end{aligned} \tag{4.4}$$

What is important, this model predictions were successfully compared with experimental data on the treatment with TNP-470, Angiostatin and Endostatin [51].

The analysis of this model dynamics for constant treatment [69] yields the following corollary.

Corollary. *If $u(t) = u$ is independent of t, then*

- *for $0 \leq u < \frac{b-\mu}{e}$ there exists a positive steady state of Eqs. (4.4), $\left(\bar{V}, \bar{K}\right) = \left(\frac{(b-\mu-eu)^{3/2}}{d^{3/2}}, \frac{(b-\mu-eu)^{3/2}}{d^{3/2}}\right)$, which is globally attractive;*
- *for $u \geq \frac{b-\mu}{e}$ there is no positive steady state and any solution tends to the trivial one $(0, 0)$.*

It should be marked that the term $-eK(t)u(t)$ in the second equation of Eqs. (4.4) is formed in the same way as the first term in the equation for $\dot{K}(t)$, that is $-\mu K(t)$, which is assumed to describe the spontaneous loss of functional vasculature [51]. Therefore, we claim that this kind of treatment modeling can be referred only to anti-vascular treatment, that is the treatment with the usage of vascular targeting agents (VTAs) which are designed to cause a rapid and selective shutdown of the blood vessels of tumors [66, 120]. In opposite to VTAs, antiangiogenic drugs are designed to inhibit the formation of new vessels on the level of signaling and therefore, treatment with their usage needs in our opinion another mathematical description. In [86] we tried to make such description by modifying the

derivation of the Hahnfeldt et. al model. We described only those antiangiogenic agents which are designed to bind and block the proteins that are responsible for inducing growth of blood vessels (*eg.* VEGF – vascular endothelial growth factor [57, 58]). An example of such agent is widely used bevacizumab (trade name Avastin, Genentech/Roche) which is a humanized monoclonal antibody that recognizes and blocks vascular endothelial growth factor A (VEGF-A) [128].

We will refer further as antiangiogenic only to the treatment that is focused on blocking the signaling of angiogenesis process, while the treatment described originally by Hahnfledt *et al.* will be referred as to antivascular.

4.2 New model derivation

The key element in introducing antiangiogenic treatment to the Hahnfeldt *et al.* model is to modify Eq. (4.3). To obtain the exact forms of both functions $S(V, K)$ and $I(V, K)$ the following diffusion–consumption equation for the concentration $n(t, x)$ of stimulators/inhibitors was used

$$\frac{\partial n(x,t)}{\partial t} = D^2 \Delta_x n(x,t) - cn(x,t) + s\mathbb{1}_{[0,r_0)}(\|x\|)\,, \tag{4.5}$$

where D^2 denotes the diffusion coefficient, c is the stimulator/inhibitor clearance rate, s is the rate of stimulator/inhibitor secretion and r_0 is the radius of the tumor, which is assumed to be a three dimensional spheroid.

We assume that administered drugs are proteins that bind and block angiogenic stimulators, and therefore we propose a modification of Eq. (4.5) (in the case when $n(x, t)$ is a concentration of stimulators) in the following form

$$\frac{\partial n(x,t)}{\partial t} = D^2 \Delta_x n(x,t) - (c + f(x, u(t)))n(x,t) + s\mathbb{1}_{[0,r_0)}(\|x\|)\,, \tag{4.6}$$

where $u(t)$ is the concentration of drug in the normal tissue at time t.

Due to the pathology of tumor angiogenesis we assume that the concentration of drug inside the tumor is different than outside, therefore we propose the following simple form of $f(x, u(t))$ function

$$f(x, u(t)) = \begin{cases} u(t) & \text{for} \quad \|x\| \in [r_0, \infty), \\ du(t) & \text{for} \quad \|x\| < r_0, \end{cases} \tag{4.7}$$

where the parameter $d \in \mathbb{R}^+$ describes the change in drug concentration caused by the incorrect structure of vessels inside the tumor.

Let us further assume that the tumor and the drug concentration are in quasi-stationary states, that is the growth rate of tumor and the change of drug concentration are small relative to the rate of distribution of factor, then

$$\frac{\partial n(x,t)}{\partial t} = 0 \quad \text{and} \quad u(t) = \text{const} = u.$$

Following [51] we assume also that concentration of stimulator is radially symmetric, that is

$$\|x\| = \|y\| \quad \Longrightarrow \quad n(x) = n(y).$$

Under those assumptions, Eq. (4.6) simplifies to the following ordinary differential equation of the second order

$$n''(r) + \frac{2}{r}n'(r) - \frac{(c + f(r,u))}{D^2}n(r) + \frac{s\,\mathbb{1}_{[0,r_0)}(r)}{D^2} = 0.$$

As in [51] we try further to obtain analytic solution of the equation formulated above. As we are interested in radially symmetric, continuously differentiable and bounded solution, we need to have the following conditions satisfied

$$n'(0) = 0 \quad \text{and} \quad \sup_{r\in[0,+\infty)} |n(r)| < +\infty\,. \tag{4.8}$$

Making the change of variables $(u, z) \to (r, n)$, where

$$\begin{aligned} u &= r\tfrac{\sqrt{c+du}}{D}, \quad z = \sqrt{r}\left(n - \tfrac{s}{c+du}\right) \quad for \quad r < r_0, \\ u &= r\tfrac{\sqrt{c+u}}{D}, \quad z = \sqrt{r}n \qquad\qquad\quad for \quad r \geq r_0, \end{aligned}$$

we obtain in both cases the modified Bessel equation in $z(u)$ of order $1/2$, from which, under the assumptions (4.8), we obtain the following form of the solution $n(r)$

$$n(r) = \begin{cases} b_1 \dfrac{D\exp\left(-r\frac{\sqrt{c+u}}{D}\right)}{r\sqrt{c+u}} & \text{for} \quad r \in [r_0, \infty), \\ \dfrac{s}{c+du} + b_2\dfrac{D\sinh\left(r\frac{\sqrt{c+du}}{D}\right)}{r\sqrt{c+du}} & \text{for} \quad r < r_0, \end{cases}$$

where b_1, b_2 are some constants. The exact expressions for b_1, b_2 are got by checking the limits

$$\lim_{r\to r_0^-} n(r) = \lim_{r\to r_0^+} n(r) \quad \text{and} \quad \lim_{r\to r_0^-} n'(r) = \lim_{r\to r_0^+} n'(r)\,.$$

Under these assumptions we obtain that

$$b_1 = \frac{s\sqrt{c_2}\exp\left(\frac{\sqrt{c_2}r_0}{D}\right)\left(\sqrt{c_1}r_0\cosh\left(\frac{\sqrt{c_1}r_0}{D}\right) - D\sinh\left(\frac{\sqrt{c_1}r_0}{D}\right)\right)}{c_1 D\left(\sqrt{c_1}\cosh\left(\frac{\sqrt{c_1}r_0}{D}\right) + \sqrt{c_2}\sinh\left(\frac{\sqrt{c_1}r_0}{D}\right)\right)},$$

$$b_2 = -\frac{\left(D + \sqrt{c_2}r_0\right)s}{c_1 D\cosh\left(\frac{\sqrt{c_1}r_0}{D}\right) + \sqrt{c_1c_2}D\sinh\left(\frac{\sqrt{c_1}r_0}{D}\right)},$$

where $c_1 = c + du$ and $c_2 = c + u$. In [51] it was assumed that c (stimulator clearance rate) is large and the exact solution $n(r)$ was approximated. In our derivation we proposed that the stimulator clearance rate is also monotonically increasing function of the drug concentration and is always greater than the clearance rate c in the absence of treatment. Therefore, we can make similar approximation as in [51] from which we obtain

$$n(r) \approx \begin{cases} \dfrac{s}{c+du} & \text{for} \quad r < r_0, \\ 0 & \text{for} \quad r \in [r_0, \infty), \end{cases}$$

Our main goal is to propose specific form of the $S(V, K)$ function under the above calculations. Therefore, we calculate the total concentration of stimulators inside the tumor

$$L(r_0, u) = \gamma \int_0^{r_0} n(r) r^2 dr \approx \gamma \frac{s}{c+du} r_0^3,$$

where γ is some constant. We see that L depends on r_0^3 and $V = \frac{4}{3}\pi r_0^3$ which yields

$$L(r_0, u) = L(V, u) \approx \frac{\alpha}{c+du} V, \quad \alpha = \tfrac{3}{4\pi}\gamma s. \tag{4.9}$$

We shall now formulate the law governing the change of drug concentration inside the tumor. We propose that it should be proportional to the inverse of the tumor volume V ($d \sim 1/(\beta + V^p)$), as the pathology is increasing during the tumor growth and decreasing due its reduction due to the treatment. Under the obtained approximation (4.9) and the assumption about the form of the change of the drug concentration we formulate the following system describing angiogenesis process with antiangiogenic treatment

$$\begin{aligned} \dot{V} &= -\varepsilon V \ln \frac{V}{K}, \\ \dot{K} &= -\mu K + b \frac{(\beta + V^p)V}{a(\beta + V^p) + u(t)} - dKV^{2/3}, \end{aligned} \tag{4.10}$$

where all parameters are non-negative.

Under the assumption that the same amount A of antiangiogenic drug is administered as bolus at time moments $t_1, \ldots, t_n$ and usual pharmacokinetic assumptions we propose the following form of $u(t)$:

$$u(t) = D \sum_{i=1}^{n} \exp\left(-clr(t - t_i)\right) \mathrm{l}_{\{t \geq t_i\}}, \tag{4.11}$$

where clr is the parameter describing the clearance rate of the drug.

4.3 Analysis of the model dynamics for constant treatment

In this section we study the behavior of the system

$$\begin{aligned} \dot{V} &= -\varepsilon V \ln \frac{V}{K}, \\ \dot{K} &= b\frac{\beta + V^p}{a(\beta + V^p) + u} V - dKV^{2/3}, \end{aligned} \tag{4.12}$$

where we assume that $\mu \equiv 0$ and $u(t) = \text{const} = u$. The first assumption follows from the estimations of parameters published in the original article [51], while the second one is the standard first attempt in analyzis of the influence of treatment.

The right-hand side of Eqs. (4.12) is properly defined in $\mathcal{D} = (\mathbb{R}^+)^2$, where $\mathbb{R}^+ = (0, +\infty)$ here. Moreover, it is of class $\mathbf{C}^1$ in $\mathcal{D}$ which yields the existence of unique solution for every initial data from $\mathcal{D}$.

Proposition. *The set $\mathcal{D}$ is invariant for Eqs. (4.12).*

Proof. Notice, that the right-hand side of Eqs. (4.12) can be extended on the boundary of $\mathcal{D}$. Indeed, for every arbitrary $K > 0$ defining

$$F_1(V) = \begin{cases} -\varepsilon V \ln \frac{V}{K} & \text{for } V > 0, \\ 0 & \text{for } V = 0 \end{cases}$$

one gets a continuous function of V. Similarly,

$$F_2(K) = b\frac{\beta + V^p}{u + a\beta + aV^p} V - dKV^{2/3}$$

is a continuous function of K for every $K \in \mathbb{R}$ and arbitrary $V \geq 0$.

Let $(V_0, K_0) \in \mathcal{D}$ be the initial point for $t_0 = 0$. We know that the unique solution exists on some time interval $[0, t^*)$. If $\mathcal{D}$ is not invariant, then there exists such initial data and time $t_1 > 0$ for which the solution reaches the boundary of $\mathcal{D}$. Therefore, either $\lim_{t \to t_1^-} V(t) = 0$ or $\lim_{t \to t_1^-} K(t) = 0$. However, the extended functions F_1 and F_2 of the right-hand side show that if $V(t_1) = 0$, then $\dot{V}(t_1) = 0$ and if $K(t_1) = 0$, then $\dot{K}(t_1) \geq 0$. Therefore, the solution to Eqs. (4.12) cannot leave the set $\mathcal{D}$. □

The general behavior of solutions of Eqs. (4.12) can be analyzed through the phase-space portrait. Analyzing the phase-space portrait we calculate the null-clines for Eqs. (4.12), that is

1. for V the null-cline in $\mathcal{D}$ is $V = K$;
2. for K the null-cline in $\mathcal{D}$ is $K = \frac{b}{d}\frac{\beta V^{1/3} + V^{p+1/3}}{a\beta + u + aV^p}$.

The dynamics of Eqs. (4.12) depends on the shape of the null-cline of $K(V)$. We see that

$$K(V) \sim \frac{b}{ad}V^{1/3}, \quad \text{as} \quad V \to \infty, \qquad K(V) \sim \frac{b\beta}{d(a\beta + u)}V^{1/3}, \quad \text{as} \quad V \to \infty.$$

we see that the null-cline of V is below the null-cline of K for small V and above this null-cline for large V. Therefore, to determine the dynamics of Eqs. (4.12) we have to determine the number of intersections between the null-cline of K and the null-cline of V, that is to calculate the number of steady states. The relation $K(V) = V$ yields

$$\alpha V^{p+2/3} + \alpha(\beta + \vartheta)V^{2/3} - V^p - \beta = 0, \tag{4.13}$$

where $\alpha = \frac{ad}{b}$ and $\vartheta = u/a$. To determine a number of positive solutions of (4.13) we use Descartes' rule of signs [3].

Although the rule can be applied only for polynomials, it is possible to use it for (4.13) with $p = k/(3n)$, $k, n \in \mathbb{N}$, since then the left-hand side of (4.13) is a polynomial of $x = V^{1/(3n)}$, and by a continuity argument the result can be extended for any $p \geq 0$.

1. For $p = 0$ the coefficients have signs: $++-$ and for $p \in (0, 2/3)$: $++--$, thus Descartes' rule of signs implies that there exists exactly one positive solution of (4.13).
2. If $p > 2/3$ we have to change the places of the second and the third term of (4.13) and then the sings are as follows: $+-+-$ and (4.13) can have either three or one positive solution.
3. In the case $p = 2/3$, the signs can be $++-$ (if $\beta + \vartheta > 1$) or $+--$ (if $\beta + \vartheta < 1$), but this means one change of sing of the coefficients, and therefore there exists exactly one positive solution to (4.13).

Now, we consider $p > 2/3$ and give a sufficient condition for the existence of a unique positive solution of (4.13). In fact, we will give a condition of the monotonicity of the left-hand side of (4.13). Differentiating with respect to V we have

$$\alpha\left(p + \frac{2}{3}\right)V^{p-1/3} + \frac{2\alpha}{3}(\beta + \vartheta)V^{-1/3} - pV^{p-1}. \tag{4.14}$$

Positivity of (4.14) for $V > 0$ is equivalent to the inequality

$$g(V) = \alpha\left(p + \frac{2}{3}\right)V^{2/3} + \frac{2\alpha}{3}(\beta + \vartheta)V^{2/3-p} > p\,, \qquad \text{for} \quad V > 0.$$

Now, we find minimum of the function g. Calculating the derivative of g and letting it to be zero we find a point V_0 at which g reaches its minimum

$$V_0 = \left(\frac{\left(p - \frac{2}{3}\right)(\beta + \vartheta)}{\left(p + \frac{2}{3}\right)}\right)^{1/p}.$$

The condition $g(V_0) > p$ guarantees monotonicity of the left-hand side of (4.13), and thus the existence of a unique positive solution of (4.13).

We can rewrite the inequality $g(V_0) > p$ and formulate the following lemma.

Lemma. *If $p \in [0, \frac{2}{3}]$ or $p > \frac{2}{3}$ and the inequality*

$$u > a\left(\left(\frac{b}{ad}\right)^{\frac{3p}{2}}\left(\frac{p + \frac{2}{3}}{p - \frac{2}{3}}\right)^{1-\frac{3p}{2}} - \beta\right) \tag{4.15}$$

holds, then there exists a unique steady state of (4.12) in $\mathcal{D}$.

We want to emphasize that Condition (4.15) is only sufficient for the existence of a unique positive steady state. If this condition is not fulfilled it can happen that the positive steady state is unique. In fact, numerical simulation suggest that three positive steady states may exist only for small values of β, and coefficients of those two additional steady states are very small.

From the phase portrait (see Fig. 4.1) it can be seen that the largest positive steady state (A) is always a stable node and so the smallest positive steady state (C), if it exists. The middle steady state, if exists, is a saddle point.

Moreover, we can formulate the following theorem.

Theorem. *If the positive steady state for Eqs. (4.12) is unique in $\mathcal{D}$, then it is globally stable in $\mathcal{D}$.*

Proof. In fact, studying the phase-space portraits for Eqs. (4.12) we see that every solution is bounded. Therefore, according to the Poincaré–Bendixson theorem any solution tends to either a steady state or to a closed orbit. However, due to the Dulac–Bendixson criterion there is no closed orbit in $\mathcal{D}$. Indeed, taking $B(V, K) = \frac{1}{VK}$ one gets

$$\frac{\partial}{\partial V}\left(-\frac{\varepsilon}{K}\ln\frac{V}{K}\right) + \frac{\partial}{\partial K}\left(\frac{b}{K}\frac{\beta + V^p}{u + a(\beta + V^p)} - dV^{-1/3}\right) = -\frac{\varepsilon}{KV} - \frac{b(\beta + V^p)}{K^2(u + a(\beta + V^p))} < 0,$$

which implies that there is no closed orbits in $\mathcal{D}$. □

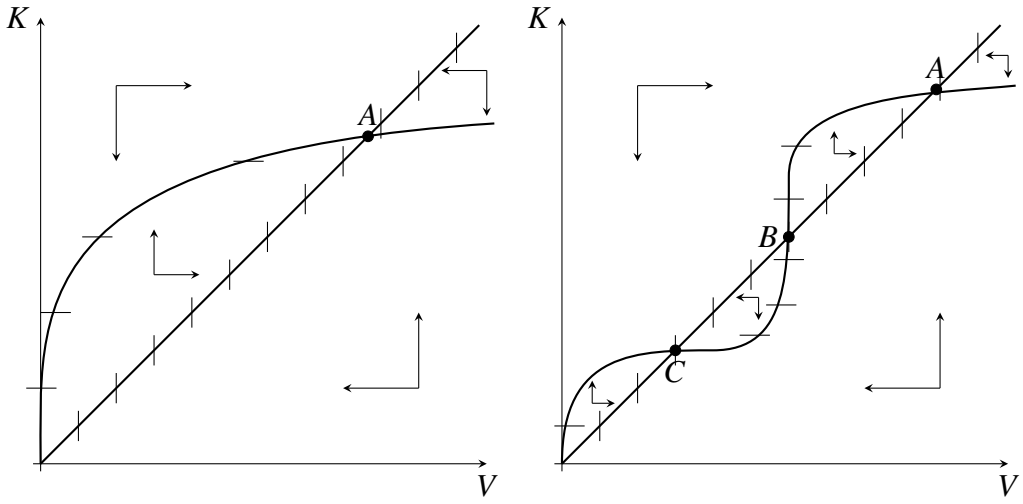

Figure 4.1: Sketch of the phase portrait of Eqs. (4.12). On the left-hand side the case with one positive steady state, and on the right-hand side the case when three steady states exist.

4.4 Numerical simulations

To illustrate the behavior of the solution of the model described by Eqs. (4.10) with the pharmacokinetic function u given by (4.11) we perform some numerical simulation. We have taken the same model parameters as Hahnfeldt *et al.* [51] rescaled as in [10]. Thus, we use the following values of the model parameters:

$$\varepsilon = 0.192\,, \quad \mu = 0\,, \quad b = 5.85\,, \quad d = 4.052\,, \quad a = 1\,, \quad e = 0.1\,, \quad \beta = 1\,.$$

The daily dose of medicine D_d varies. In fact, we use $D = D_d/n$, where n is the number of doses applied each day. If the medicine is applied every kth day, then $n = 1/k$. For chosen parameters' values there exists a unique positive steady state of Eqs. (4.12).

In order to compare the treatment that is considered in the original Hanhnfeldt model with the treatment proposed by us we use exactly the same pharmacokinetic function.

We have compared the solution of the original Hahnfeldt *et al.* model with the modified model for $p = 1$ (see Figs. 4.2, 4.4, 4.6) and the modified model for different values of p, this is for $p = 2$ and $p = 0$ (see Figs. 4.3, 4.5, 4.7).

If the treatment is applied rarely an oscillation due to application of the medicine can be observed (see Figs. 4.2, 4.3, 4.4, 4.5, 4.6, 4.7). If the daily dose is small, the size of tumor in the stationary state is smaller for the modified model than for the Hahnfeldt *et al.* model and deceases with decreasing p (see

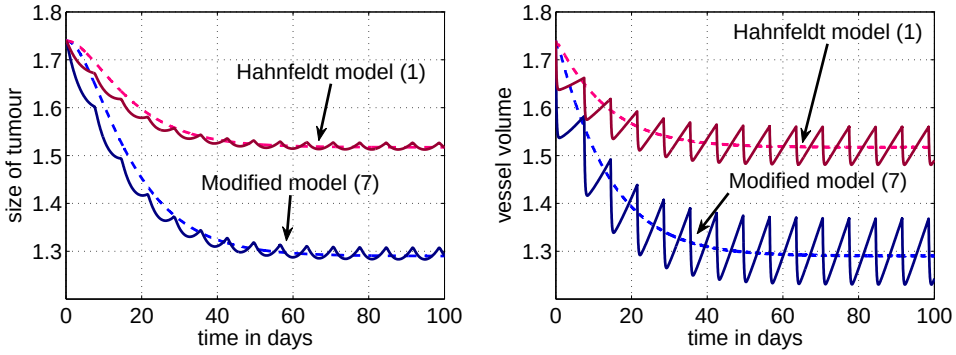

Figure 4.2: Comparison of solutions of the Hahnfeldt model (4.4) and modified model (4.10) for daily dose 0.05. Solid line – the solution for a dose is applied one a week, dotted line – a dose is applied every hour.

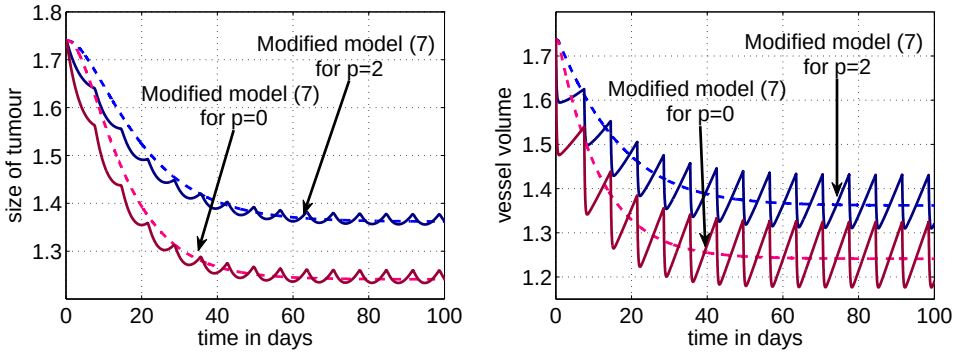

Figure 4.3: Comparison of solutions of the modified model (4.10) for daily dose 0.05 for different values of p. Solid line – the solution for a dose is applied one a week, dotted line – a dose is applied every hour.

Fig. 4.2, 4.3 and 4.8). If the daily dose is larger, the size of tumor in the stationary state become smaller with increasing p (see Fig. 4.4, 4.5 and 4.8). For daily dose large enough (larger than 0.5), the size of tumor in the steady state becomes smaller for the Hahnfeldt *et al.* model (see Fig. 4.6, 4.7 and 4.8).

We have not observed any significant difference in means of the solutions for various treatment regimes when means were calculated over the interval equal to the time between doses' applications.

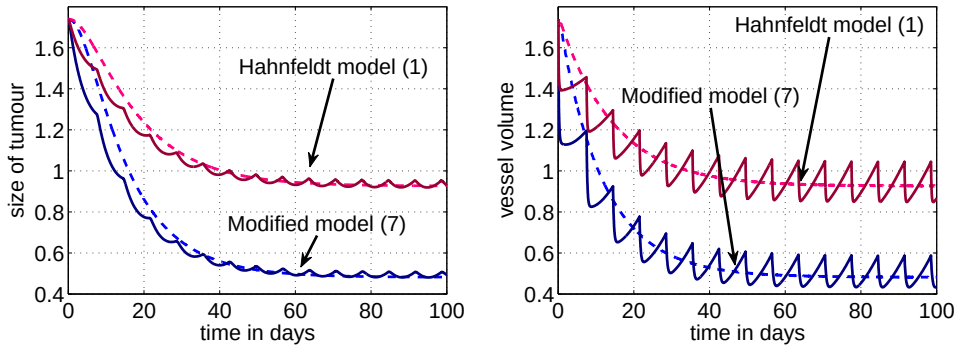

Figure 4.4: Comparison of solutions of the Hahnfeldt model (4.4) and modified model (4.10) for daily dose 0.2. Solid line – the solution for a dose is applied one a week, dotted line – a dose is applied every hour.

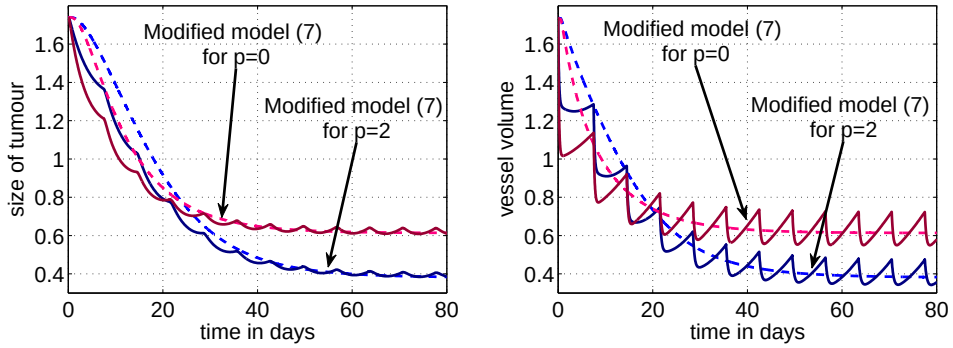

Figure 4.5: Comparison of solutions of modified model (4.10) for daily dose 0.2 for different values of p. Solid line – the solution for a dose is applied one a week, dotted line – a dose is applied every hour.

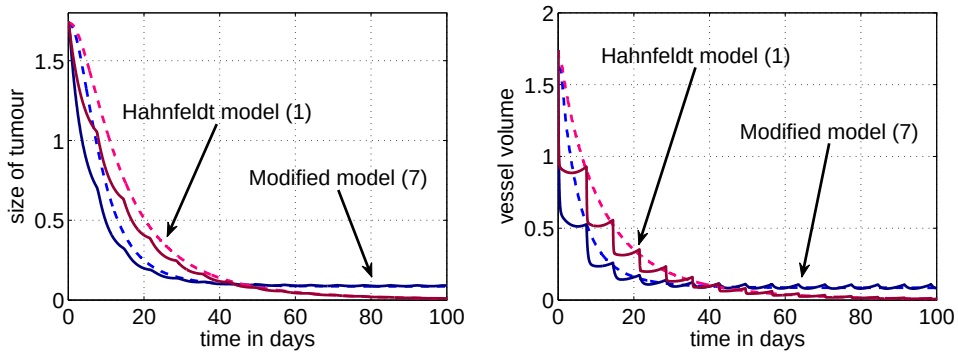

Figure 4.6: Comparison of solutions of the Hahnfeldt model (4.4) and modified model (4.10) for daily dose 0.7. Solid line – the solution for a dose is applied one a week, dotted line – a dose is applied every hour.

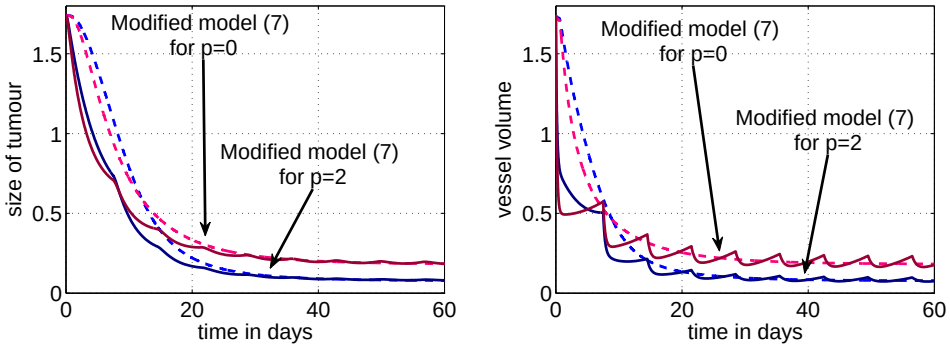

Figure 4.7: Comparison of solutions of modified model (4.10) for daily dose 0.7 for different values of p. Solid line – the solution for a dose is applied one a week, dotted line – a dose is applied every hour.

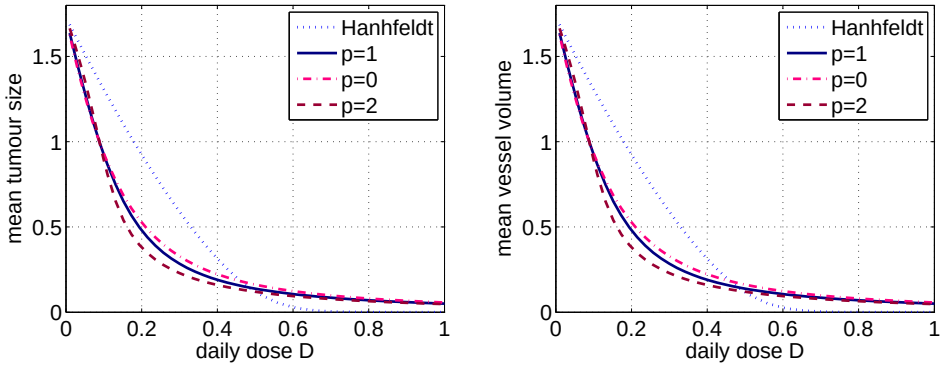

Figure 4.8: Comparison of the mean value of the solution to the Hahnfeldt model (4.4) (dotted line) and modified model (4.10) (solid line) in the stationary state (after long time) for depending on daily dose

4.5 Summary

In this chapter we have described a new approach to antiangiogenic treatment. Typically, such treatment is described as a separate term in the equation describing the dynamics of vessels' volume, as in the case of the classical Hahnfeldt *et al.* model [51]. In our opinion such term reflects anti-vascular treatment, while anti-angiogenic treatment occurs on the level of the angiogenic signaling. We have considered such type of drugs which acts on the stimulators of angiogenesis and therefore, basing on the Hahnfeldt *et al.* ideas [51] we have modified the term describing stimulation of angiogenesis. As it can be expected, the dynamics of both considered models is completely different. Starting the research on antiangiogenic treatment Folkman [43] believed that this should lead to complete

recovery from cancer disease. Therefore, there were such requirements for the Hahnfeldt *et al.* model that it should reflect complete recovery for sufficiently high drug dosage. Now, after many years of experiments we know that generally it is not true. This is reflected in our modified model. We have studied the dynamics of the modified model in the case of constant treatment. We know that for the original Hahnfeldt *et al.* model the complete recovery is guaranteed under the assumption of sufficiently high drug dosage. For the modified model we have shown that complete recovery is impossible independently of the magnitude of this dosage; this phenomenon was noticed in [35, 37]. This suggest that using only anti-angiogentic treatment we are not able to cure cancer. However, using anti-angiogenic treatment we are able to decrease both cancer and vessels' volume and normalize vasculature such that chemotherapy can better penetrate tumor mass. This is now the main goal of anti-angiogenic treatment. We have performed a series of numerical simulations using non-constant treatment, described as an application of drug as bolus. As for the constant treatment, the application of the same doses of drugs give different results depending on the Hill coefficient p. In our opinion, experiments with different doses of different drugs should be performed in order to check which model is better for the description of the specific drug.

Chapter 5

Optimal control

This Chapter presents results of the research on anti-angiogenic treatment in the context of optimal control. It is prepared on the basis of [91], in which we summarized the results of our research on that topic. Cancer treatment using the anti-angiogenic agents targets the evolution of tumor vasculature. The aim is to significantly reduce supplies of oxygen and nutrients, and thus starve the tumor and induce its regression. We consider the family of tumor angiogenesis models proposed by Hahnfeldt *et al.* described by Eqs. (4.1)-(4.2) together with our modification – Eqs. (4.10), that increases accuracy in the case of treatment using VEGF antibodies. Our aim is to consider the optimal control problem of minimizing the tumor volume when the maximal admissible drug dose (the total amount of used drug) and the final level of vascularization are also taken into account. We investigate the solution of that problem for a fixed therapy duration. We show that the optimal strategy consists of the drug-free, full-dose and singular (with intermediate values of the control variable) intervals. Moreover, no bang-bang switch of the control is possible, that is the change from the no-dose to full-dose protocol (or in opposite direction) occurs on the interval with the singular control. For two particular form of the models, used by Hahnfeldt *et al.* and Ergun *et al.*, we provide additional theorems about the optimal control structure. We investigate the optimal controls numerically using the customized software written in MATLAB ®, which we make freely available for download (http://labpages.moffitt.org/enderlingh/jan/) and attach its source in Appendix A. Utilized numerical scheme is based on the composition of the well known gradient and shooting methods.

5.1 Introduction

Conventional cancer therapies, such as radiotherapy or chemotherapy, are designed to induce large amount of cell death in rapidly proliferating cancer cells. Although such therapies are capable of shrinking the tumor many orders of magnitude, the complete tumor eradication is often unachievable [72]. In addition, cancer cells may acquire drug resistance, because of their fast duplications combined with high genetic instability. Novel treatment approaches shift focus away from the cancer cells and instead target the environment that supports the tumor [14]. An example of such approach is the antiangiogenic therapy postulated by Folkman [43], which is designed to inhibit the vascular support of the tumor, and thus induce the tumor starvation and regression. It holds the promise of being less patient specific, because it targets genetically stable host vasculature and not the constantly mutating tumor cells [23]. Moreover, it has been proposed that the proper dose of the antiangiogenic drugs might significantly improve chemotherapy efficacy [57, 58]. Namely, without the treatment, tumor has the ability to recruit new blood vessels in a process called tumor angiogenesis. However, it has been discovered that tumor angiogenesis is highly pathological – incorrect structure and poor efficiency of newly formed vessels are common tumor features [57, 58]. Some trials revealed that those vasculature pathologies result in significant impairment of the chemotherapy delivery since most of the administered drug dose is not even absorbed by the tumor and the successfully delivered part is not distributed uniformly in the tumor region [57]. The hypothesis is that the proper amount of antiangiogenic drugs may cause in the removal of abberant neovessels (in a process called vascular pruning) what would result in the increase of the overall vasculature quality, and thus in the boost of chemotherapy efficacy through its increased delivery. Of course too high dose of the agents may destroy too much of the tumor vasculature, leading to the poor drug delivery. Hence, the effort is to identify the dosage and the timing of the normalization window caused by the antiangiogenic therapy in order to increase the efficacy of chemotherapy.

Here, we address the problem of designing optimal protocols for the antiangiogenic treatment. We focus our attention on the therapeutic agents directly blocking angiogenesis inducing proteins which are secreted by the cancer cells (compare bevacizumab, trademark Avastin®, that inhibits vascular endothelial growth factor VEGF). We base our analysis on the well established family of mathematical models originating from the Hahnfeldt *et al.* model of tumor angiogenesis [51]. However, we consider the models with the modification proposed in [86] which was introduced in order to better reflect the effect of con-

sidered drugs and, to our knowledge, has never been analyzed from the optimal control point of view. We consider the optimal control problem of minimizing the tumor volume for a fixed therapy duration and when the maximal admissible drug dose, the total amount of used drugs, and the final level of vascularization (ratio of the carrying capacity to the tumor volume) are also taken into account. We explicitly introduce the part of the payoff functional describing the level of final vascularization in order to capture the concept of vasculature related to chemotherapy efficacy, what, to our knowledge, is also a novelty. Our main aim is to formulate as much detailed description of the optimal control as possible.

5.2 Considered family of tumor angiogenesis models

The family of models proposed by Hahnfeldt at el. described by Eqs. (4.1)-(4.3) was extensively used in the context of optimal control. In current studies it is usually assumed that the main goal of the antiangiogenic treatment is to minimize the tumor volume at the end of treatment, compare Świerniak *et al.* [111, 117] or Ledzewicz and Schättler [68, 69]. Various constraints on the treatment protocol are considered, among them: limited total amount of drug, maximal admissible dose or fixed therapy duration. For the original Hahnfeldt *et al.* model it has been shown that with limited amount of drug, fixed maximal drug dose and without fixed therapy duration the maximal minimization of tumor is achieved in a very non-trivial way [68, 69]. More precisely, the optimal treatment strategy might consist of a singular control interval in which the dosage depends on the temporal tumor volume and vasculature size. However, for a fixed duration of antiangiogenic therapy and for the Ergun *et al.* and d'Onofrio and Gandolfi forms of the model (see Tab. 4.1 in Chapter 4) the structure of optimal control is much simpler [112]. Namely, the intermediate doses of the drug are not optimal, and thus the optimal protocol has a bang-bang structure, that is it consists of switches between maximal dose and no drug intervals. Nowadays much effort is put into optimizing the combined treatments, *i.e* protocols in which antiangiogenic drugs are administered simultaneously with chemotherapy/radiotherapy. Various combined treatment protocols have been intensively studied through numerical simulations [33, 92] or from the optimal control point of view [60, 113, 114]. Numerical investigations show that there is an increase in the chemotherapy efficiency when antiangiogenic agents are simultaneously administered [92].

Let us recall that in Chapter 4 we have proposed new idea of antiangio-

genic treatment modelling. In [86] we argued that the original model, although successful in predicting the response to many therapeutic agents, might insufficiently describe the effect of antiangiogenic drugs that directly inhibit angiogenic stimulating molecules. Bevacizumab (trademark Avastin®), a humanized monoclonal antibody, that inhibits vascular endothelial growth factor A (VEGF-A), was provided as an example of such agent [86]. For the antiangiogenic agents with the course of action comparable to bevacizumab, the following modification of the original model (Eqs. (4.1) and (4.3)) was proposed

$$\begin{aligned} \dot{V}(t) &= -\varepsilon V(t) \ln \frac{V(t)}{K(t)}, \\ \dot{K}(t) &= -\mu K(t) + \frac{l}{a+u(t)} S(V(t), K(t)) - dI(V(t), K(t)), \end{aligned} \tag{5.1}$$

which is from one hand a generalization of Eqs. (4.10) derived in Chapter 4, because in (4.10) we have specific forms of the function S and I, but from the other hand it is a specific case of Eqs. (4.10) for $p = 0$. Note that in comparison to the original model the treatment does not induce gross reduction of vasculature but selectively inhibits the formation of tumor-stimulated neovasculature. What is important, comparisons of the modified and original models predictions with the experimental data show that when Bevacizumab is applied as the therapeutic agent, then the quality of fit is higher (data approximation error is lower) for the modified model [85, 88].

In the following, we consider only the family of models described by Eqs. (5.1) with continuously differentiable functions $S(V, K)$ and $I(V, K)$. For a particular kind of functions describing inhibition and stimulation, we can show positivity of solutions of Eqs. (5.1). More precisely, the following lemma holds.

Lemma. *If $I(V, 0) = 0$ and $\forall V \geq 0\ S(V, 0) \geq 0$, then the solution of Eqs. (5.1) remains positive for positive initial data, independently of the maximal admissible dose of drug.*

Proof. Indeed, the first equation of Eqs. (5.1) can be rewritten in the integral form

$$V(t) = V(0) \exp\left(-\varepsilon \int_0^t \ln \frac{V(s)}{K(s)} ds \right).$$

Hence, $V(0) > 0$ implies $V(t) > 0$ for all $t > 0$. Let us further assume that $K(t) \to 0$ as $t \to t_1$ for some $t_1 > 0$. However, from the second equation of Eqs. (5.1) we have that $\dot{K}(t_1) = \frac{l}{a+u} S(V, 0) \geq 0$ due to the positivity of V. Hence, uniqueness of solutions yields their positivity for the positive initial data. □

Lemma 5.2 is crucial for the next Section, as the strict positivity of solutions of Eqs. (5.1) is constantly used. Notice, that the assumptions of Lemma 5.2 are fulfilled for all formulas presented in Tab. 4.1.

5.3 Results

The main part of the payoff functional that we consider in our minimization problem has a standard form and is consisted of the tumor volume at the end of therapy, $V(T)$, and the total amount of the used drug $\int_0^T u(t)dt$, where T is the fixed therapy duration. However, we would also like to tackle the problem of subsequent (after the antiangiogenic therapy) chemotherapy administration. According to the "vessels normalization" hypothesis, efficient treatment with chemotherapy is possible only when the cytotoxic agent can be distributed evenly, that is when vessels penetrate most of the tumor regions and have the proper structure and functionality [58]. In order to reflect that phenomena, we assume that the higher the tumor vascularization (defined as the ratio of the vessels carrying capacity to the tumor volume, $K(t)/V(t)$) is, the larger the chemotherapy efficacy is. Hence, we take into account the tumor vascularization at the end of the treatment and we assume the following form of the payoff functional

$$P[u(\cdot)] = V(T) - k_1 \frac{K(T)}{V(T)} + k_2 \int_0^T u(t)dt\,, \tag{5.1}$$

where $T > 0$ is the treatment duration, and $k_1\,,\ k_2$ describe the trade-offs between separate treatment goals. Additionally, the cumulative side effects of the chemotherapeutic agents are taken into account to measure the side effects of the treatment. Hence, a penalty term in the form of integral to the terminal time T is present in the considered payoff functional. Clearly, $\int_0^T u(t)dt$ measures the total amount of the given cytotoxic agent u. Moreover, because of the high cost of anti-angiogenic agents one can not give indefinite administrations of the agents. Thus, we assume that the total amount of the anti-antiangiogenic agents is limited by A_{max}, i.e.

$$\int_0^T u(t)dt \leq A_{max}.$$

Our goal is to minimize $P[u(\cdot)]$ subject to the dynamics of Eqs. (5.1) for the fixed therapy duration T and over all measurable functions $u : [0,T] \to \left[0, \tilde{A}\right]$, where $\tilde{A}$ denotes the maximal drug dose that can be administered without making a harm to the patient. Clearly, we do not consider the model describing the

influence of the chemotherapy and thus, although it seems biologically reasonable, we cannot claim that the usage of the final vascularization in the payoff functional is an optimal way for combined protocol in which we assume that the chemotherapy is administered after the antiangiogenic treatment. In fact, the optimality strongly depends on the way in which the chemotherapy is incorporated into the model.

Before analyzing the problem in details, we discuss the optimal treatment protocol when the only goal is to minimize the tumor volume at the end of the therapy, i.e. when $k_i = 0$ for $i = 1, 2$.

Lemma. *If $k_1 = 0$ and $k_2 = 0$, then the optimal treatment protocol for Eqs. (5.1) is to give the maximal admissible dose through the whole treatment interval, that is $u_*(t) \equiv \tilde{A}$.*

Proof. Suppose that the optimal control $u_*(t)$ for Eqs. (5.1) is less than $\tilde{A}$ on some interval of non-zero Lebesgue measure. Then there exists $t^* < T$ such that $K_*(t) > K_f(t)$ for $t > t^*$, where $K_*(t)$ and $K_f(t)$ are the second coordinates of the solutions corresponding to the optimal control u_* and the full-dose protocol $u_f(t) \equiv \tilde{A}$, respectively. It easily follows that $V_*(T) > V_f(T)$, and hence $u_*(t)$ is not an optimal control. □

Clearly, if we focus only on minimizing the tumor volume, then the structure of optimal treatment protocol is straightforward. This scenario can be utilized when the antiangiogenic treatment is administered just before the tumor resection. In such a case the final vascularization and the total amount of used drug can be omitted.

We consider now the structure of optimal control for strictly positive values of k_1 and k_2. Let us denote the right-hand side of Eqs. (4.10) by $F(V, K, u)$. The part of the payoff functional P that depends only on the endpoint can be treated as a function of $(V(T), K(T))$, that is $G(V(T), K(T)) = V(T) - k_1 \dfrac{K(T)}{V(T)}$. From the Pontryagin Minimum Principle it follows that if $u_*(t)$ is an optimal control and $(V_*(t), K_*(t))$ is the corresponding trajectory, then there exists a function (adjoint or co-state variable) $y : [0, T] \to \mathbb{R}^2$, which satisfies the adjoint system of equations $\dot{y} = -D^T_{(V,K)} F \cdot y$, where $D_{(V,K)}F$ describes the Jacobi matrix of F with respect to V and K, with the terminal condition $y(T) = \nabla G(V(T), K(T))$, and such that Hamiltonian $H(y, V, K, u) = y^{\mathrm{T}} F(V, K, u)$ is minimized [18, 93].

In our case the adjoint variables satisfy the following system of ordinary

differential equations

$$\begin{aligned}\dot{y}_1 &= \varepsilon y_1\left(\ln\frac{V_*}{K_*}+1\right) - y_2\left(\frac{l}{a+u_*}\frac{\partial S(V,K)}{\partial V}\bigg|_{(V_*,K_*)} - d\frac{\partial I(V,K)}{\partial V}\bigg|_{(V_*,K_*)}\right),\\ \dot{y}_2 &= -\varepsilon y_1\frac{V_*}{K_*} + y_2\left(\mu - \frac{l}{a+u_*}\frac{\partial S(V,K)}{\partial K}\bigg|_{(V_*,K_*)} + d\frac{\partial I(V,K)}{\partial K}\bigg|_{(V_*,K_*)}\right),\end{aligned} \tag{5.2}$$

with the terminal conditions

$$\begin{aligned}y_1(T) &= 1 + k_1\frac{K_*(T)}{(V_*(T))^2} > 0\,,\\ y_2(T) &= -k_1\frac{1}{V_*(T)} < 0\,,\end{aligned} \tag{5.3}$$

and the optimal control $u_*(t)$ together with the corresponding trajectories $(V_*(t), K_*(t))$ and $(y_1(t), y_2(t))$ minimizes the Hamiltonian H given by

$$H(y_1, y_2, V, K, u) = -\varepsilon y_1 V\ln\frac{V}{K} - y_2\Big(\mu K - \frac{l}{a+u}S(V,K) + dI(V,K)\Big) + k_2 u\,.$$

Moreover, as the Hamiltonian does not depend explicitly on t, its value is constant on the optimal trajectory

$$H(y_1, y_2, V_*, K_*, u_*) \equiv \text{const}\,.$$

Through the minimization property on the Hamiltonian H the function

$$\Phi = \frac{\partial H}{\partial u} = H_u = k_2 - \frac{l}{(a+u)^2}y_2 S(V,K)\,, \tag{5.4}$$

determines the structure of the optimal control $u_*(t)$. Since the stimulation term $S(V,K)$ is positive for positive V and K, we have that if the co-state variable y_2 is negative or equal to zero, then $\Phi > 0$. Hence, from minimization property we have that $u_* = 0$ for $y_2 \le 0$. For positive values of y_2 there always exits $\bar{u} = \sqrt{\frac{l}{k_2}y_2 S(V,K)} - a$ such that $\Phi = 0$. If $\bar{u} \in [0, \tilde{A}]$, then $u_* = \bar{u}$, since $H_{uu} > 0$ for any value of u. Similarly, if $\bar{u} < 0$ ($\bar{u} > \tilde{A}$), then $u_* = 0$ ($u_* = \tilde{A}$). Thus, the values of the control are determined by the co-state y_2 and (V,K) as follows:

$$u_*(t) = \begin{cases} 0 & \text{for } y_2 \le 0\,,\\ \min\{\max\{\sqrt{\dfrac{l}{k_2}y_2 S(V,K)} - a\,,\ 0\}\,,\ \tilde{A}\} & \text{for } y_2 > 0\,.\end{cases} \tag{5.5}$$

As it can be seen, there are singular parts of the control, but the intermediate values of the optimal u can be calculated explicitly. Moreover, it is clear that

the switch from the full-dose to no-dose protocol (or in the opposite direction) can occur only through singular interval and not in a bang-bang manner. In addition, since the terminal condition for y_2 is negative, y_2 remains negative in some neighborhood of T. Formula (5.5) implies that this neighborhood is the drug free interval, and hence we may state the following lemma.

Lemma. *Optimal control for Eqs.* (5.1) *ends with the drug free interval* $(\tau, T]$.

In general, because of the constrains on the control value, we can have multiple intervals in which $u_* = 0$ or $u_* = \tilde{A}$ for $y_2 > 0$. However, in the next subsection we provide theorems limiting the number of points in which the change of the sign of y_2 occurs. Let us denote the intervals in which $y_2 > 0$ by "y" and in which $y_2 \leq 0$ (drug free intervals) by "0".

5.3.1 Case of functions considered by Ergun *et al.*

For the stimulatory and inhibitory functions considered by Ergun *et al.* the adjoint equation for the co-state variable y_1 reduces to the following

$$\dot{y}_1 = \varepsilon y_1 \left(\ln \frac{V_*}{K_*} + 1 \right).$$

Hence, if y_1 vanishes at some $\bar{t}$, then $y_1 \equiv 0$ for all $t > \bar{t}$ as a consequence of the uniqueness of solutions of Eqs. (5.2). Therefore, it cannot change the sign and the terminal condition (5.3) implies that y_1 is strictly positive for all t. As the time derivative of the co-state variable $y_2(t)$ at point $y_2(t) = 0$ is equal to

$$\dot{y_2}(t)\Big|_{y_2(t)=0} = -\varepsilon y_1 \frac{V_*}{K_*},$$

and only the switch of the y_2 sign can occur. Thus, we may formulate the following theorem.

Theorem. *For Eqs.* (5.1) *with* $S(V, K) = K^{2/3}$ *and* $I(V, K) = K^{4/3}$ *there is at most one switch of the* y_2 *sign during the whole treatment interval, i.e. the optimal control is at most* $y\,0$.

5.3.2 Case of functions considered by Hahnfeldt *et al.*

Assume that $l - \mu a > 0$. This means that for the therapy free model considered by Hahnfeldt *et al.* [51], that is when $u \equiv 0$ in Eqs. (5.1), there exists a single globally asymptotically stable positive steady state $(\bar{V}, \bar{K})$, cf. [10, 34]. Thus, we consider a successfully growing tumor, which cannot be eliminated without the

treatment. Phase portrait analysis (see Fig. 5.2) allows to prove the following lemma.

Lemma. *In the absence of therapy ($u = 0$), the set $\mathcal{D} = \{(V, K) \in \mathbb{R}^+ : V < \bar{V}, K < \bar{K}\}$, where $(\bar{V}, \bar{K})$ is the positive steady state, is positively invariant for Eqs. (5.1) with $S(V, K) = V$, $I(V, K) = KV^{2/3}$ and $l > \mu a$.*

The number of points in which the change in the y_2 sign can occur is limited by the following theorem.

Theorem. *For Eqs. (5.1) with $S(V, K) = V$, $I(V, K) = KV^{2/3}$, $(V(0), K(0)) \in \mathcal{D}$ and $l > \mu a$ there are at most two switches of the y_2 sign during the whole treatment interval, that is the optimal control is at most $0\,y\,0$.*

Proof. Assume that there are three or more switches of the y_2 sign in the whole treatment interval. The derivative of the co-state variable y_2 at the switch point is expressed as

$$\dot{y_2}(t)\Big|_{y_2(t)=0} = -\varepsilon y_1 \frac{V_*}{K_*}.$$

Hence, if $y_1 > 0$, then the y_2 switches from positive to negative values. If $y_1 < 0$, then the switch occurs in the opposite direction. In order to get more than one switch of the optimal control, y_1 needs to change the sign from negative to positive in the interval in which $y_2 > 0$, compare Fig. 5.1. At the switching

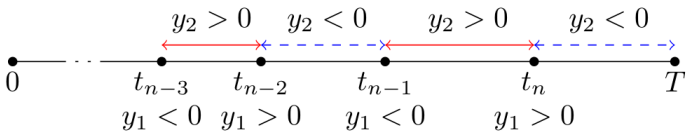

Figure 5.1: Structure of the optimal control. Moments t_i denote the y_2 switching points. Blue dashed lines denote no-dose intervals.

points, that is when $y_2 = 0$, we have

$$H(y_1, 0, V_*, K_*, u_*) = -\varepsilon y_1 V_* \ln \frac{V_*}{K_*},$$

and as the Hamiltonian is constant, we obtain that if at any switching point $y_1 < 0$ and $V_* > K_*$ ($V_* < K_*$), then $V_* < K_*$ ($V_* > K_*$) if $y_1 > 0$ at any other switching point.

Let us focus now on the switch from the singular to no-dose protocol that occurs before the last one of that type (t_{n-2} in Fig. 5.1). In order to have that switch,

y_1 should change its sign from positive to negative during the treatment free interval, that is in the interval in which $y_2 < 0$ (the interval (t_{n-2}, t_{n-1}) in Fig. 5.1). Hence, at some point inside this interval the following inequality should be satisfied

$$\dot{y}_1\Big|_{y_1=0} = -y_2\left(\frac{l}{a} - d\frac{2}{3}\frac{K_*}{V_*^{1/3}}\right) < 0\,.$$

This inequality is equivalent to

$$K_* > \frac{3l}{2ad}V_*^{1/3}. \tag{5.6}$$

In the treatment free model (Eqs. (5.1) with $u(t) \equiv 0$), the null-cline for the variable K is described by the following equation

$$K = \frac{\frac{l}{a}V}{\mu + dV^{2/3}}\,,$$

and if Inequality (5.6) is satisfied at some (V_*, K_*), then it is easy to see that (V_*, K_*) lies above the null-cline for the variable K, that is (V_*, K_*) is placed in the area C in Fig. 5.2, while we consider only the set $\mathcal{D}$. On the other hand,

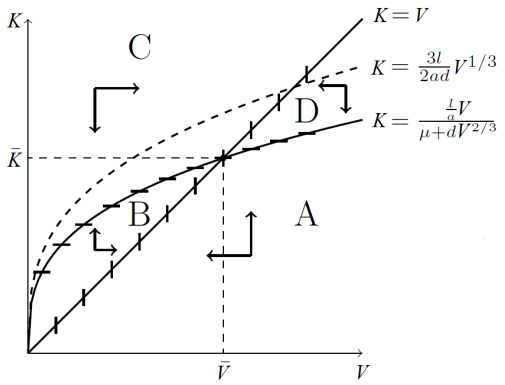

Figure 5.2: Sketch of the phase portrait.

from the structure of the optimal control we have that during the same therapy free interval the ratio of the tumor volume to the carrying capacity V_*/K_* should start below (above) 1 and end above (below) 1. Looking at the phase portrait in Fig. 5.2 we see that if the solution starts below the null-cline $K = V$, that is from the area A, then it either remains in the same area or moves from A to B and remains in B. In that case Inequality (5.6) cannot be fulfilled and there cannot be a second switch of the optimal control from the full-dose to no-dose protocol. If the solution starts above the null-cline $K = V$, that is initially $K_* > V_*$, then it remains above that null-cline and it is impossible to have $K_* < V_*$ at the end of the interval. This completes the proof. □

For the stimulatory and inhibitory functions considered by d'Onofrio and Gandolfi [34], that is for $S(V,K) = K$ and $I(V,K) = KV^{2/3}$, we were unable to formulate any theorem limiting the number of y_2 sign switches.

5.4 Numerical results

There are various methods that allow to approximate numerically the optimal control for given parameters and initial conditions [82, 125]. For the purpose of this paper we implemented numerical scheme based on two well known methods: gradient (steepest descent) method and shooting method. The former one uses the information about the derivative of the Hamiltonian with respect to the control and can be summarized in the following steps:

1. Pick a control $\tilde{u}$ and solve the model equations (5.1) for $(\tilde{V}(t), \tilde{K}(t))$.
2. Integrate adjoint equations (5.2) backwards using terminal conditions (5.3) with $(\tilde{V}(T), \tilde{K}(T))$. Calculate simultaneously $\frac{\partial H}{\partial u}$.
3. Pick k such that the control $\bar{u} = \tilde{u} - k\frac{\partial H}{\partial u}$ gives a smaller value of the payoff functional. Proceed to 1 with $\tilde{u} = \bar{u}$.

The above procedure ends when the change in the payoff functional reaches prescribed tolerance. What is important, the gradient method gives rapid initial convergence. However, much faster final convergence is obtained with the shooting method, which is also less computationally intensive [82] and can be summarized in the following steps:

1. Pick an initial condition for the adjoint equations (5.2) and solve them together with the model equations (5.1) with the control u calculated using information about the $\frac{\partial H}{\partial u}$.
2. Calculate the error between the obtained terminal conditions and the ones that should be fulfilled (5.3).
3. Adjust the initial condition in order to decrease the absolute value of the calculated error (use for example the Newton-Raphson method) and proceed to 1.

We decided to use the combination of those two methods. Namely, we utilize the gradient method with relatively large prescribed tolerance to generate initial condition for the shooting method. All procedures are written in MATLAB® computing language and we share their source code on our personal websites and

the sourceforge.net repository. What is important, we already implemented angiogenesis models (see Tab. 4.1) in both modified and original forms. Moreover, necessary modifications of the code in case of other stimulation and inhibition functions are simple and straightforward. Hence, the code gives a good basis for other numerical investigations of optimal antiangiogenic treatment protocols.

5.4.1 Numerical approximation of the optimal controls

Values of the parameters associated with the optimal control settings were taken arbitrary and the only criterion was that all of the terms in the payoff functional should be significant. For the therapy duration T equal to 30 days and the initial condition $(V(0), K(0)) = (3000\,mm^3, 4000\,mm^3)$ we set $k_1 = 10^3$ and $k_2 = 5$ or $k_2 = 100$ depending on the simulation. For the maximal admissible dose we set $\tilde{A} = 20\,mg/kg$ since it was the maximal dose used in one of the Bevacizumab related experiments [85]. In the numerical simulations we consider the stimulation and inhibition functions considered by Hahnfeldt *et al.* and Ergun *et al.* as both of them were fitted to Bevacizumab data in [85, 88] and we take the estimated parameters values as presented in Tab. 5.1.

First, we numerically investigate the optimal control problem for the Ergun *et al.* form of the modified model (5.1). We take the smaller value of k_2, that is we consider the case in which the influence of the total amount of used drug on the overall performance is smaller, compare Eq. (5.1). Numerical solution to that optimization problem is presented in the Fig. 5.3. It can bee seen that, as stated

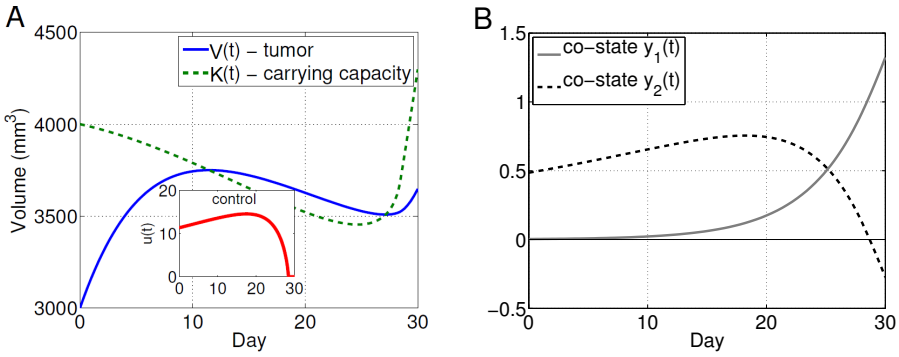

Figure 5.3: Optimal treatment strategy for the Ergun *et al.* model. (A) Solution to the model (4.10) with the optimal control u presented in the inset. (B) Corresponding dynamics of the co-state (adjoint) variables (5.2).

in Lemma 3, the optimal control ends with a short drug-free interval. Moreover, for the rest of the treatment interval it is singular, that is u takes the intermediate dose values. This result completely agrees with the analysis carried out in

Parameter	Description	Unit	Ergun *et al.*	Hahnfeldt *et al.*
ε	*tumor growth rate*	day^{-1}	0.2032	0.074
μ	*rate of spontaneous loss of functional vasculature*	day^{-1}	0	0.002
l	*l/a is the rate of vessels growth stimulation*	$\text{day}^{-1}\text{conc}$	10.39	2.8109
a		conc	4.598	2.1008
d	*rate of endogenous inhibition of previously generated vasculature*	$\text{day}^{-1}\text{vol}^{-2/3}$	0.0028	0.002

Table 5.1: Model parameters used in all numerical simulations. Values for Hahnfeldt *et al.* and Ergun *et al.* models are taken from [85] and [88], respectively.

the previous section. Interestingly, singular control never reaches the maximal admissible dose ($\tilde{A} = 20\,mg/kg$) and one can see that the shape of the optimal control is similar to the dynamics of the y_2 co-state variable, compare panel A and B in Fig. 5.3. The later behavior of the control is related to the relatively small changes in the tumor volume during the treatment course, and hence the changes in y_2 have larger impact on the formula used to calculate u, compare Eq. (5.5).

Similar shape of the optimal control can bee also seen for the Hahnfeldt *et al.* model, compare Fig. 5.4(A). However, for the same value of the parameter k_2 there is an additional interval in which the full-dose protocol is realized, showing that the additional non-singular intervals are possible. Another non-singular no-

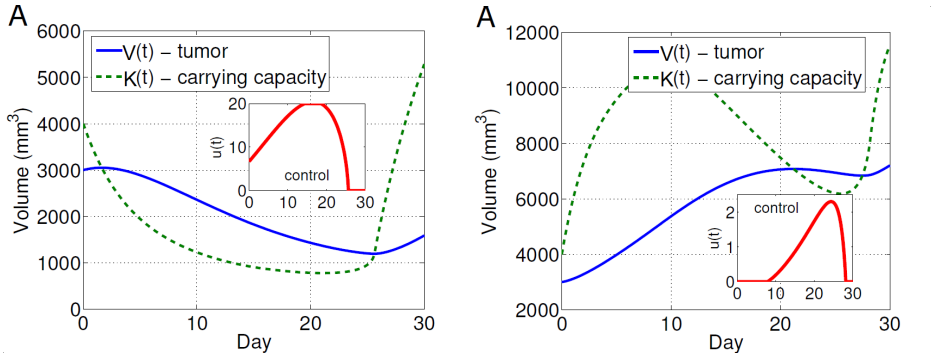

Figure 5.4: Optimal treatment strategy for the Hahnfeldt *et al.* model with $k_2 = 5$ (A) and $k_2 = 100$ (B). Presented are the solutions to the model (5.1) together with the corresponding optimal controls u presented in the insets.

dose interval appears in the case of $k_2 = 100$, that is when there is higher penalty for using antiangiogenic drugs, see Fig. 5.4(B). Interestingly, the additional no-dose interval occurring before the singular one is realized with $y_2 > 0$ and on its left there is a tiny interval with the singular control appearing again (not visible in the plot inset).

5.5 Summary

Investigating the influence of new cancer therapies on tumor development is of the great importance. Their effects, both when used as supportive and stand alone therapies, need to be verified. In this Chapter we addressed the problem of designing optimal protocols for the antiangiogenic treatment using therapeutic agents directly blocking angiogenesis inducing proteins, such as VEGF. We based our analysis on the well established family of mathematical models originating from the Hahnfeldt *et al.* model of tumor angiogenesis [51]. We considered those models with the modification proposed in [86]. Moreover, we introduced additional part to the standard payoff functional that describes the level of final vascularization, what, to our knowledge, is also a novelty. Proposed modification of the payoff functional tackles the "vessels normalization" hypothesis, which states that efficient treatment with chemotherapy is possible only when the cytotoxic agent can be distributed evenly, that is when vessels penetrate most of the tumor regions and they have proper structure and functionality. Namely, if the chemotherapy is administered after the antiangiogenc treatment, then it seems biologically reasonable to have as much vascularized tumor as possible before chemotherapy.

We have shown that the optimal strategy consists of the drug-free, full-dose and singular (with intermediate values of the control variable) intervals. What is important, we have shown that even for the fixed treatment duration T the singular controls are the common feature of the whole considered family of models. Singular controls in cancer treatment were previously obtained only for particular angiogenesis models [68, 69] and for some chemotherapy models [116]. From the structure of the optimal controls it follows that no bang-bang switch of the control is possible, i.e. there is no change from the no-dose to full-dose protocol (or in opposite direction) on the interval with the singular control. For Hahnfeldt *et al.* and Ergun *et al.* models, we provided additional theorems about the optimal control structure.

Finally, we investigated the optimal controls numerically using the customized software written in MATLAB ®, which we made freely available for download from our personal websites. Utilized numerical scheme is based on the composition of the well known gradient (steepest descent) and shooting methods. Numerical simulations showed clearly that the structure of the optimal controls are far from being simple and they can have multiple switches from the no-dose to singular to full-dose regimes.

Chapter 6

Sensitivity analysis

Last Chapter is devoted to another practical issue – sensitivity analysis of angiogenesis models in the context of anti-angiogenic treatment, and is based on my research with the group of Heiko Enderling and Philip Hahnfeldt, published in [89]. We study the effects of parameter value uncertainties for a model of tumor development under angiogenic signaling for two different treatments: anti-vascular and anti-angiogenic. We consider the classical Hahnfeldt *et al.* model and our modification described in detail in Chapter 4. Data fitting is performed to compare predictions of both models and to obtain nominal parameter values for sensitivity analysis. Sensitivity analysis reveals that the success of different cancer treatments depends on tumor size and tumor intrinsic parameters. In particular, we show that tumors with ample vascular support can be successfully targeted with conventional cytotoxic treatments. On the other hand, tumors with curtailed vascular support are not limited by their growth rate and therefore interruption of neovascularization emerges as the most promising treatment target.

6.1 Introduction

Anti-angiogenic treatment is designed to inhibit the tumor vascular support and thus increasing oxygen tension and inducing tumor cell starvation. This can be achieved either by targeting the neo-vasculature directly or by interfering with pro-angiogenic factors secreted by the tumor [66]. Anti-angiogenic treatment holds the promise of being less patient-specific as the host vasculature is targeted and not the constantly evolving tumor population [23]. We compare two different anti-angiogenic agents by local and global sensitivity analysis of parameters describing tumor-vasculature interactions. We utilize models described in

previous Chapters, that is the Hahnfeldt *et al.* model described by Eqs. (4.4) and the modified model proposed by us (4.10). The local sensitivity analysis investigates the effect of small variation in a single parameter about its nominal/average value when all other parameters are kept fixed at the estimated values. However, biological systems contain typically substantial variations in almost all parameters values; between patients and even within tumors of a single patient. Hence, it might happen that the model parameter a is locally the most influential for one patient, while for another patient (with other set of nominal parameters values) it is parameter b. In contrast, a global sensitivity analysis reveals which parameters are the most influential in general by perturbing all parameters simultaneously, assuming patient population heterogeneity and thus parameter values uncertainty.

The model proposed by Hahnfeldt *et al.* (Eqs. (4.4)) can simulate the effect of anti-angiogenic treatment, and model predictions were successfully compared with experimental data of treatment with TNP-470, Angiostatin and Endostatin [51]. We shall refer to this models as 'the original model'. Additionally, we consider the model without treatment described by Eqs. (4.1)-(4.2), which will be referred as to 'control'.

As we have pointed out in Chapter 4 the original model, although successful in predicting the response to therapeutic agents that block the growth of new blood vessels (for example, Angiostatin), might insufficiently describe the effect of anti-angiogenic drugs that act to inhibit angiogenic stimulation. Bevacizumab, a humanized monoclonal antibody that inhibits vascular endothelial growth factor A (VEGF-A), was provided as an example of such agent [86]. For anti-angiogenic agents like Bevacizumab we proposed Eqs. (4.10) instead of Eqs. (4.4). Note that in comparison to the original model, treatment does not induce gross reduction of vasculature but selectively inhibits formation of tumor-stimulated neovasculature. In this Chapter we consider the simplest version of Eqs. (4.10) with $p = 0$. This is also a specific form of Eqs. (5.1) exploited in Chapter 5, namely for S and I considered by Hahnfeldt *et al.* We shall refer to that model as 'the modified model' describing the response of a tumor to anti-angiogenic treatment.

Both models (4.4) and (4.10) should be equipped with the description of the time dependent concentration of an administered inhibitor $u(t)$. Under the usual pharmacokinetic assumptions [13], instead of discrete formula (4.11) presented in Chapter 4, in the following we assume that $u(t)$ is expressed as

$$u(t) = \int_0^t c(s) \exp\big(- clr(t-s)\big) ds \tag{6.1}$$

where $c(s)$ is the administration rate at time s and clr is the clearance rate of the considered inhibitor.

6.1.1 Data fitting

Data fitting of control, original and modified models was performed to experimental data obtained by Fujita and colleagues [48]. The values estimated in the original model [51] were taken as the initial set of parameters for tumor growth without treatment, i.e., the control case. The maximal perturbation value for each parameter was assumed to be equal to 80% of its initial value. For spontaneous death rate μ, which was neglected in the original model analysis, we assumed the range of admissible values between 0 and 1 (representing 0%–100%). For treatment associated parameters D, clr and e, we only considered positive values. Data fitting was divided into control case fitting and subsequent treatment model fitting. In both cases, trust region method (incorporated in MATLAB lsqnonlin function) for finding the minimal fit error values was utilized. The trust-region-reflective algorithm uses a quadratic approximation for the minimized function (defined by the first two terms of its Taylor approximation) in a neighborhood (trust region) around the current point x to improve the current approximation error [15]. In order to avoid finding only local minima we generated 1000 random initial parameter values for the optimization procedure.

6.1.2 Sensitivity analysis

We focused on the sensitivity of tumor volume V and ignored the sensitivity of effective vascular support K (as V is directly dependent on K). Local sensitivities were obtained by solving the extended system of equations and taking the derivative of the initial vector field with respect to all parameters. To measure global sensitivity we assumed that each parameter is perturbed by a uniformly distributed random variable within the range of ±10% or ±20% of the initial parameter value. Spearman's partial rank correlation coefficients were calculated from 1000 samples generated with a Latin Hypercube Sampling (LHS) algorithm [77]. The scatter plots of obtained samples revealed only monotonic relations between tumor volume and parameters. The sensitivity indices, defined as fraction of total output variance generated by the uncertainty in the respective parameter value, were calculated using the Fourier Amplitude Sensitivity Test (FAST) method [28].

6.2 Results

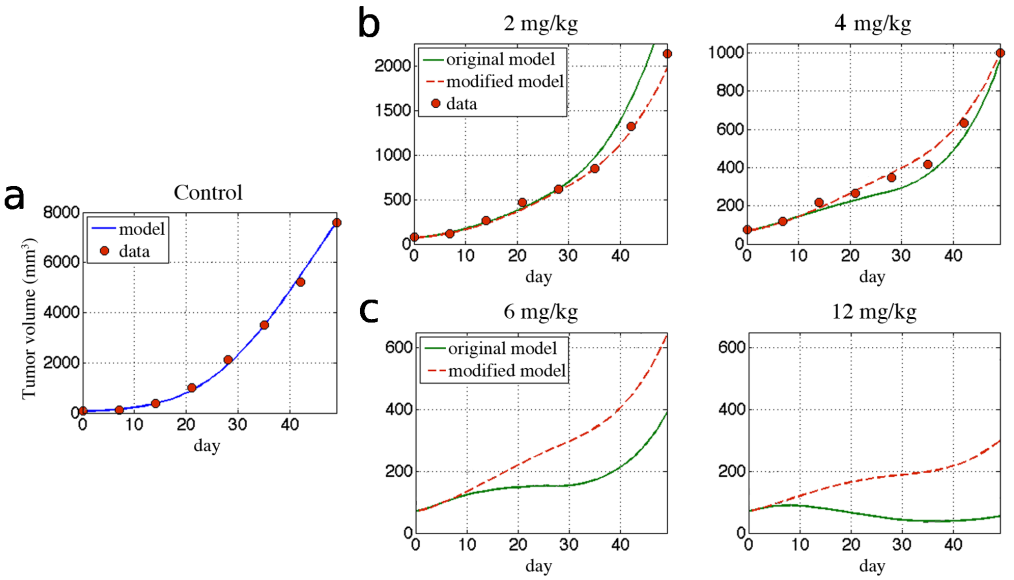

Figure 6.1: Fitted model curves and predicted tumor response to different doses of bevacizumab. Control data derived from [48] and parameters in Table 1. (a) Control data and the fitted model curve using Eqs. (4.1)-(4.2). (b) Treatment data together with the solutions to original (Eqs. (4.4)) and modified (Eqs. (4.10)) models. (c) Response of tumor for higher doses of bevacizumab: 6 mg/kg and 12 mg/kg

6.2.1 Bevacizumab treatment data

The impact of Bevacizumab on head and neck squamous cell tumors grown in Female BALB/c nu/nu nude mice was investigated experimentally [48]. Tumor-bearing mice were randomized at mean tumor volume 50-100 mm^3. Mice were treated with Bevacizumab either 2 mg/kg/day or 4 mg/kg/day on days 1 and 4 of each week for 4 weeks. Both treatment regimes were shown to decelerate growth but are insufficient to prevent tumor expansion (Fig. 6.1b).

Although Bevacizumab was not injected as bolus, for simplicity we assume that $c(s) = D(\delta(s - t_1) + \delta(s - t_2) + \ldots)$, where D is the administered dose and t_i are the injection days. This assumption may generally lead to decrease in fit quality but should not influence the comparison between considered models. Comparison of the experimental data with fitted curves demonstrates the ability of both models to reproduce the experimental data (Fig. 6.1a). An excellent control fit was obtained when solving the model (Eqs. (4.1)-(4.2)) for parameters

ε, μ, b and d (Fig. 6.1a). In contrast to previous assumptions that spontaneous vasculature loss μ is negligible [51] we obtained the best fitting curve for $\mu > 0$, specifically $\mu = 0.0021$ (cf. Table 1). This value, however, is relatively small and therefore its role in the model will be addressed in the next sections. A good fit for early response to low doses of Bevacizumab of 2 and 4 mg/kg/day was obtained by both the original and modified model without significant differences in tumor growth curves (Fig. 6.1b). At the end of the treatment ($t > 30$ days), however, the original model fails to correctly approximate tumor growth for the 2 mg/kg/day treatment. For both doses of Bevacizumab the total fit error for the modified model was about two times smaller than for the original model (1.78 for 2 mg/kg/day and 1.75 for 4 mg/kg/day of Bevacizumab), see Table 1 for specific values of fit error. Large differences in treatment predictions by both models are observed for higher doses of bevacizumab (Fig. 6.1c). For treatment doses of 12 mg/kg/day, the original model predicts a more than three times larger tumor response to treatment than the modified model. Due to lack of data for such a high doses of Bevacizumab, however, we are unable to score the model predictions.

6.2.2 Treatment free model: sensitivity analysis

Parameter values obtained in the previous subsection describe average tumor growth. Each parameter, however, has an intrinsic burden of uncertainty, which is reflected in patient-specific clinical disease courses of tumors of the same organ. In order to obtain the compact form of the considered models, however, many aspects of the tumor angiogenesis process have been incorporated into single parameters, which introduces additional variation in their values. Sensitivity analysis for the treatment-free model described by Eqs. (4.1)-(4.2) demonstrates the influence of the uncertainty in the parameters values (Fig. 6.2). A basic approach to measuring sensitivity at a fixed time point is to calculate the partial derivatives of systems solution with respect to the parameters [100]. That 'local' sensitivity analysis provides direct information on the effect of small variation in a single parameter about its nominal value. Our analysis revealed that variation in the parameter for spontaneous loss of vasculature, μ in Eq. (4.2), has no significant influence on the tumor size (Figure 2) and can therefore be neglected in the model as predicted by Hahnfeldt *et al.* [51]. Sensitivity analysis further shows that for early tumor growth up, i.e. $t < 50$ days, there is no significant difference in 'local' sensitivity to each parameter (Fig 6.2a). In other words, small variation in each single model parameter has similar impact on early tumor growth dynamics. After $t = 50$ days, however, when the tumor has reached an apprecia-

	Description	Control	Original model	Modified model
e	drug impact		0.0636	0.4755
clr	clearance rate		0.0745	0.0799
ε	growth rate	0.0741	0.0741	0.0741
μ	loss of vessels	0.0021	0.0021	0.0021
b	stimulation	1.3383	1.3383	1.3383
d	inhibition	0.002	0.002	0.002
V_0	initial V	71.2553	71.2553	71.2553
K_0	initial K	71.6675	71.6675	71.6675
Fit error	average %	6.57	2 mg/kg/day: 12.66;	2 mg/kg/day: 7.1;
	per point		4 mg/kg/day: 10.97	4 mg/kg/day: 6.26

Table 6.1: Estimated tumor growth parameters. The kinetic model (Eqs. (4.1)-(4.2)) was applied first to the untreated control tumor data, and the growth parameters ε, μ, b, d, and K_0 (initial value of K) were solved for by performing gradient-based optimization for 1000 randomly chosen set of initial parameters. Using obtained parameters the data for Bevacizumab (2 or 4 mg/kg) was used to solve for the respective treatment parameters e and clr in case of the original model (Eqs. (4.4)) and the modified model (Eqs. (4.10)).

ble size, sensitivity to growth rate ε begins to decrease while sensitivity to other model parameters continues to increases at similar rates as before. Therefore, tumor growth for larger tumors is not determined by its intrinsic growth rate but increasingly dependent on parameters associated with the angiogenesis process.

Although the performed local analysis provides direct information on the effect of small parameter perturbations about their nominal values, it does not indicate the effect of concurrent, large perturbations in all model parameters. In cancer progression and treatment, many parameters are unknown or only estimated, and may be uncertain by one or more orders of magnitude [100]. In order to reflect this uncertainty, we assume that the value of each parameter is uniformly distributed around the nominal value obtained through data fitting in previous

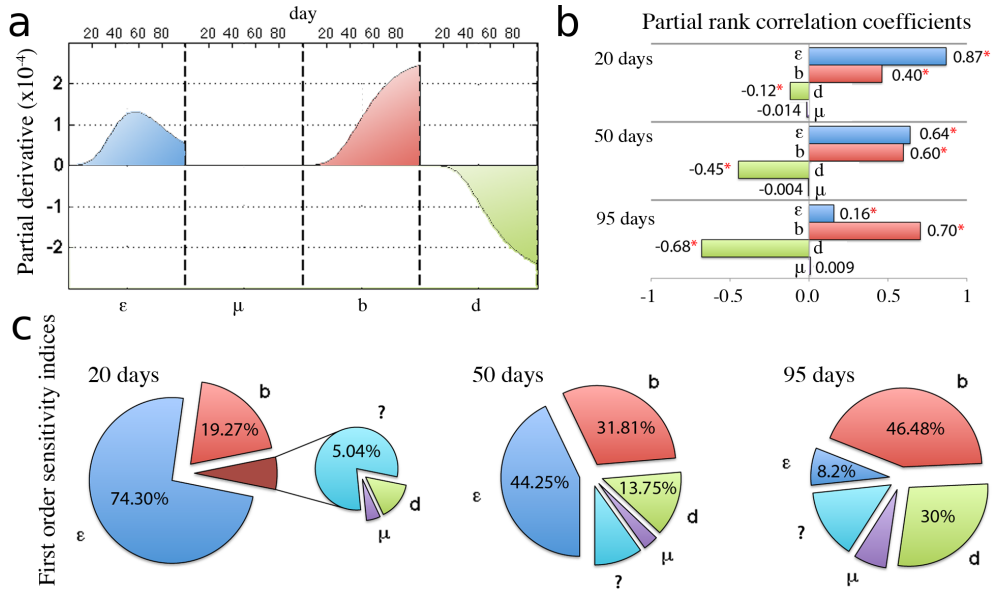

Figure 6.2: Local and global sensitivity analysis for the control case. Analysis carried with the nominal parameters values presented in Table 1. (a) Time evolution of the local sensitivities, defined as the partial derivatives of the tumor growth curve taken with respect to each parameter and multiplied by the nominal parameter value. (b) Partial rank correlation coefficients between each parameter and the tumor volume after 20, 50 or 95 days from initiation. Coefficients were calculated from 1000 randomly generated samples under the assumption that each parameter is uniformly varied by no more than 10% of its initial value ($*$ denotes p-value below 0.01). (c) First order sensitivity indices, defined as the fraction of the total variance in tumor volume caused by the variation in each parameter value. Calculations were performed after 20, 50 and 95 days from tumor initiation using the FAST method and under the assumption that parameters are varied uniformly by no more than 10%.

section. We set the range of that distribution to ±10% of the nominal value. Such amount of uncertainty in each parameter yields up to 30% differences in the tumor volume 100 days after initiation. Figure 6.2 b and c show the partial rank correlation coefficients and variance decomposition indicative of most influential parameters perturbations. At large tumor sizes local and global sensitivity analysis concur that tumor progression is most sensitive to angiogenesis-associated parameters. Global sensitivity analysis, however, reveals that tumor growth rate ε is the major determinant of tumor progression when the tumor is small (Fig. 6.2c). At the beginning of tumor growth almost 75% percent of variation in tumor volume are due to uncertainty in the tumor growth rate. Similar size dependence is confirmed in the values of partial rank correlation coefficients

(Fig. 6.2b). The initial high correlation of tumor volume with the value of the tumor growth rate decreases in favor of angiogenesis-associated parameters. From the global sensitivity analysis we derive the following therapeutic implications:

(i) at small tumor sizes it is better to perturb the tumor growth rate by targeting cancer cells directly;

(ii) manipulation of the vascular supply by increasing inhibition or decreasing stimulation is the most promising approach when tumors have grown to a substantial size.

6.2.3 Target angiogenic stimulators or endothelial cells?

As alluded to above, anti-angiogenic drugs can have different courses of action. One class of drugs interferes with the balance of angiogenesis promoters and inhibitors in favor of inhibition, whereas the other class prevents blood vessel formation regardless of stimulatory signals. We set out to answer the question which anti-angiogenic mechanism is less patient specific and promises more robust treatment results. The original model is used in case of Angiostatin, TNP-470 and Endostatin and the modified model for Bevacizumab. Table 2 shows the pharmacokinetic parameters for Bevacizumab as estimated above (cf. Table 6.1), as well as TNP-470, Angiostatin and Endostatin as estimated by Hahnfeldt and colleagues through fitting to experimental data [48]. We assume the same treatment protocol as in the previous section with drugs being administered on days 1 and 4 of each week for 4 weeks. Doses for TNP-470, Angiostatin and Endostatin are chosen to give response curves comparable to treatment with Bevacizumab at 4 and 8 mg/kg/day. For sensitivity analysis of the treatment model we only present data for Angiostatin as similar results were obtained for both TNP-470 and Endostatin (data not shown).

In order to investigate the robustness of the treatment outcome we revisit the intrinsic uncertainty for parameters ε, μ, b, d, e. We assume that the variation is uniformly distributed around the nominal value of the parameter and its maximal value is limited to 20%. Figure 6.3 shows the global sensitivity analysis revealing the influence of parameter uncertainty on tumor volume 26 days after initiation. For both drug dose regimes a larger variation in tumor volume is observed for Angiostatin than for Bevacizumab. With comparable average tumor volumes at the end of treatment, Bevacizumab yields 34% and 49% lower standard deviation from average tumor size than Angiostatin for both lower and higher drug doses, respectively. The minimal tumor volumes for both drug regimes however, are in favor of Angiostatin, with almost 25% less tumor volume than the small-

est tumors obtained with Bevacizumab. On the other hand, the worst possible outcomes (maximal tumor volume) with Bevacizumab were almost 30% smaller than those in the Angiostatin group. The decomposition of the variance revealed no significant differences between both drugs, providing the similar amount of unexplained origin of variation (higher order interactions) (compare Fig. 6.3c). Differences are only observable in the dependence of tumor volume on uncertainty in parameter d describing endogenous vasculature inhibition. Estimated partial rank correlation coefficients show higher correlation of d with treatment outcome for Bevacizumab, suggesting that tumors with larger endogenous inhibition of tumor angiogenesis may respond better to Bevacizumab.

	e **(drug impact)**	clr **(clearance rate)**	D **(dose)**
TNP-470	1.3	10.1	13.2; 20.2
Endostatin	0.66	1.7	4.1; 5.8
Angiostatin	0.15	0.38	4.2; 5.9
Bevacizumab	0.4755	0.0799	4; 8

Table 6.2: Dosage of different agents giving similar therapeutic effects. Shown are the exact values of pharmacokinetic parameters (e, clr) and doses (D) for which the original model (TNP-470, Endostatin, Angiostatin) and the modified one (Bevacizumab) give the same tumor volume at the end of treatment. Values of pharmacokinetic parameters, except for Bevacizumab, were estimated in [7].

6.3 Discussion

Mathematical models can be utilized to dissect complex mechanisms underlying tumor growth and response to treatment, especially if treatment is not directed at tumor cells but at the environment that modulates tumor growth kinetics. We set out to investigate the sensitivity of parameters in a well-studied mathematical model of tumor growth with reciprocal dependence on its vascular support, and its response to anti-angiogenic treatment [51, 86]. In line with previous assumptions, our analysis confirmed that tumor growth rate as well as tumor-orchestrated angiogenesis promotion and inhibition outweigh spontaneous loss of vasculature in tumor growth dynamics. Local and global sensitivity analysis

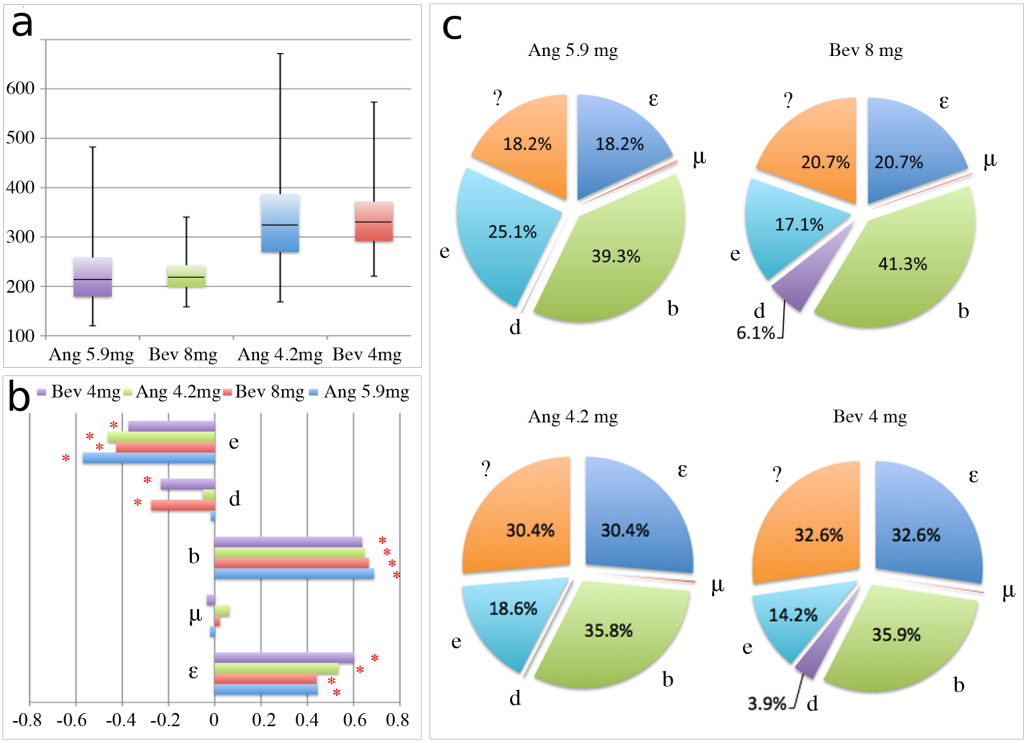

Figure 6.3: Global sensitivity analysis for Bevacizumab and Angiostatin. Analysis carried for two different dose regimes and with the nominal parameters values presented in Tables 6.1 and 6.2. (a) Box plot of tumor volume after 26 days from the initiation calculated from 1000 samples generated under the assumption that parameters ε, μ, b, d, e are varied uniformly up to 20%. (b) Partial rank correlation coefficients between each parameter and the tumor volume after 26 days from initiation ($*$ denotes p-value below 0.01). (c) First order sensitivity indices, defined as the fraction of the total variance in tumor volume caused by the variation in each parameter value. Calculations were performed after 26 days from tumor initiation using the FAST method.

further revealed that tumor growth is separated into distinct phases with different dependence on underlying mechanisms. Intuitively, when a tumor is initiated its progression is predominantly determined by the intrinsic growth rate, that is, ratio of cell proliferation to cell death. As the tumor grows and exhausts its vascular support the growth rate becomes insignificant and tumor progression is increasingly dependent on the interplay of angiogenesis promoting and inhibiting mechanisms. These findings offer valuable insights into tumor size-dependent treatment design. Small tumors as well as tumors progressing with ample vascular support might be best targeted by direct induction of cell kill. Tumors with curtailed vascular support are not dependent on their growth rate,

and induction of cell kill will only have minimal effects. We showed that for such tumors interference with the neovascularization is the most promising treatment target. These model predictions will need to be confirmed in carefully designed animal experiments that allow for quantification of the degree of tumor vascularization and vascularization-dependent response to cytotoxic and anti-angiogenic treatments as well as their combinations.

A number of anti-angiogenic treatments have recently been approved for both single treatment and in combination with other therapeutic agents and many more are in various stages of clinical trials. The Hahnfeldt model has successfully predicted tumor response to anti-angiogenic treatment with TNP-470, Angiostatin and Endostatin [51]. A modification of that model put forward by Poleszczuk *et al.* extended its applicability to treatment with Bevacizumab [86]. We normalized treatment protocols in both models to achieve comparable tumor sizes after treatment and analyzed the sensitivity of both models to the underlying parameters. With equal perturbation of parameters in both models representative of patient variability we showed that the average tumor sizes after treatment with both Angiostatin and Bevacizumab are similar. The deviation from average response, however, was significantly larger for Angiostatin, indicating that the course of action with Bevacizumab is less patient specific and thus wider applicable. The most favorable outcome, however, was observed for treatment with Angiostatin, with final tumor size being more than 30% smaller than the best sample from the Bevacizumab group. On the other hand, the least successful treatment outcome featured also a significantly larger tumor in the Angiostatin group compared to Bevacizumab. No significant differences in parameter sensitivity were found between both drugs, providing similar amount of unexplained origin of variation in tumor response. These results visualize that higher order interactions between tumor, vasculature and anti-angiogenic agents are at play that are yet to be fully deciphered.

In conclusion, we have demonstrated that simple mathematical models with a small number of experimentally validated parameters can reliably reproduce and predict tumor growth and treatment response data. Thorough analysis of parameter uncertainty yields invaluable insights into mechanisms driving growth kinetics and response of tumors. Our study encourages the measure of tumor vasculature as a surrogate for tumor carrying capacity as a biomarker, which may ultimately lead to better-informed patient-specific synergizing of cytotoxic and anti-angiogenic treatment. These findings from our analysis augment the understanding of cause-action relation of tumor kinetics and aim to drive future experiments and clinical validation towards improved understanding and ultimately patient prognosis.

Chapter 7

Summary

In the war with cancer even slight improvement in the efficacy of currently approved therapeutic agents is of great importance. Taking into account more than 8 million cancer related deaths in 2012 alone, improvement of already approved cancer therapies by 1% translates into 80,000 saved lives. In the thesis I have focused on the secondary effects that can be caused by the radiotherapy, which is one of the most widely used cancer therapies. I stated a novel hypothesis that radiation induces cellular senescence outside the irradiated field, which in turn triggers tumor angiogenesis leading to fast growth of previously existing subclinical tumor sites. Thus, I postulated that adding adjuvant anti-angiogenic therapy to radiotherapy could improve the overall treatment outcome.

In the first part of the thesis, I focused on preliminary verification of the considered hypothesis using *in vitro* experiments. Together with the group of my co-supervisor Prof. Maria Wideł we performed a series of experiments, in which we irradiated both cancer and non-transformed human cell lines and quantified the amount of induced senescence. Results clearly show that the bystander signals can induce senescent phenotype in bystander non-irradiated populations. This effect, however, is dependent on the TP53 gene status – in the considered co-incubation periods it was detected only for cells having a functioning p53 protein. Those results indicate that senescence can be indeed induced in cells residing outside of the MRI outlined irradiation field. However, considered hypothesis needs additional experimental verification, which will be the focus of further research. First step will be to perform experiments in which directly irradiated cancer cells will be co-incubated with non-irradiated non-transformed cells. That setting will be closer to the *in vivo* setting as most of the cells outside of the irradiation field are non-transformed. In the subsequent experiments we

will also measure concentration of vascular endothelial growth factor (VEGF) to make sure that the angiogenesis can be indeed triggered in the non-irradiated tissue. Ultimate verification of the considered hypothesis, however, can be made only in clinical trials, which are outside of the scope of this thesis. However, even before attempting to design a clinical trial or murine experiment, one needs to know the dosage at which the anti-angiogenic drug should be applied. That problem can be tackled using mathematical models, which can be calibrated using experimental and clinical data.

That is why in the second part of the thesis, I focused on the mathematical modeling of tumor angiogenesis process and its response to anti-angiogenic treatment. In the research conducted together with the group of my supervisor Prof. Urszula Foryś, we have focused on modeling the effect of the drugs that act on the stimulators of angiogenesis. Developed mathematical framework is based on the well recognized model proposed by Hahnfeldt in [51] and, in contrary to the original model, predicts that complete disease remission is impossible independently of the magnitude drug dosage; this phenomenon was noticed in [35, 37]. This suggest that using only anti-angiogentic treatment we are not able to cure cancer. However, using anti-angiogenic treatment we are able to normalize vasculature such that chemotherapy can better penetrate tumor mass, which is now the main outcome studied for anti-angiogenic treatment.

That outcome of the treatment has been analyzed as an optimal control problem in the third part of the thesis. Together with the group of Prof. Urszula Foryś we have introduced additional part to the standard payoff functional that describes the level of final vascularization, what, to our knowledge, is also a novelty. Using Pontryagin Minimum Principle we have shown that the optimal strategy consists of the drug-free, full-dose and singular (with intermediate values of the control variable) intervals. What is important, we have shown that even for the fixed treatment duration the singular controls are the common feature of the whole considered family of models. In order to be able to calculate optimal treatment schedules on a per-patient basis in the future trials, we have written numerical procedures approximating optimal controls, which we made freely available for download from our personal websites. Utilized numerical scheme is based on the composition of the well known gradient (steepest descent) and shooting methods.

In the final chapter of the thesis I focused on another practical issue – sensitivity analysis of angiogenesis models in the context of anti-angiogenic treatment. Presented research, focused on comparing the outcomes of treatment using anti-vascular and anti-angiogenic drugs, has been conducted with the group of Heiko Enderling and Philip Hahnfeldt. With equal perturbation of parameters

in both models, representative of patient variability, we showed that the average tumor sizes after treatment with both anti-vascular and anti-angiogenic drugs are similar. The deviation from average response, however, was significantly larger for anti-vascular drugs, indicating that the course of action with anti-angiogenic drugs is less patient specific and thus wider applicable.

Results presented in this thesis provide firm background for future research, hopefully leading to performing clinical trial informed by the mathematical models. Mathematically informed clinical trials are the new fast developing field in cancer research, giving hope for deciphering large complexity of tumor biology and ultimately wining the war with cancer.

Bibliography

[1] Z. Agur, L. Arakelyan, P. Daugulis, Y. Ginosar. Hopf point analysis for angiogenesis models. *Discrete and Continuous Synamical Systems B*, 4(1):29–38, 2004. [citation on page 28]

[2] B. Alberts, D. Bray, K. Hopkin, A. Johnson, J. Lewis, M. Raff, K. Roberts, P. Walter. *Essential cell biology*. Garland Science, 2013. [citation on page 11]

[3] B. Anderson, J. Jackson, M. Sitharam. Descartes' rule of signs revisited. *American Mathematical Monthly*, 5(105):447–451, 1998. [citation on page 35]

[4] L. Arakelyan, V. Vainstein, Z. Agur. A computer algorithm describing the process of vessel formation and maturation, and its use for predicting the effects of anti-angiogenic and anti-maturation therapy on vascular tumor growth. *Angiogenesis*, 5(3):203–214, 2002. [citation on page 28]

[5] C. M. Beauséjour, A. Krtolica, F. Galimi, M. Narita, S. W. Lowe, P. Yaswen, J. Campisi. Reversal of human cellular senescence: roles of the p53 and p16 pathways. *The EMBO Journal*, 22(16):4212–4222, 2003. [citation on page 14]

[6] E. H. Blackburn, J. G. Gall. A tandemly repeated sequence at the termini of the extrachromosomal ribosomal RNA genes in Tetrahymena. *Journal of Mathematical Biology*, 120(1):33–53, 1978. [citation on page 13]

[7] B. J. Blyth, P. J. Sykes. Radiation-induced bystander effects: what are they, and how relevant are they to human radiation exposures? *Radiation Research*, 176(2):139–57, 2011. [citation on page 4 and 15]

[8] M. Bodnar, U. Foryś. Hahnfeldt angiogenesis model with time delays. *Proceedings of the XIII National Conference on Applications of Mathematics in Biology and Medicine*, pages 18–23, 2007. [citation on page 28]

[9] M. Bodnar, U. Foryś. Angiogenesis model with carrying capacity depending on vessel density. *Journal of Biological Systems*, 17(1):1–25, 2009. [citation on page 28]

[10] M. Bodnar, U. Foryś. Influence of time delays on the Hahnfeldt et al. angiogenesis model dynamics. *Applicationes Mathematicae (Warsaw)*, 36(3):251–262, 2009. [citation on page 37 and 50]

[11] M. Bodnar, M. J. Piotrowska. Stability analysis of the family of tumour angiogenesis models with distributed time delays. *Communications in Nonlinear Science and Numerical Simulation*, 31(1-3):124–142, 2016. [citation on page 28]

[12] M. Bodnar, M. J. Piotrowska, U. Foryś, E. Nizińska. Model of tumour angiogenesis — analysis of stability with respect to delays. *Mathematical Biosciences and Engineering*, 10(1):19–35, 2013. [citation on page 28]

[13] P. L. Bonate, J.-L. Steimer. *Pharmacokinetic-pharmacodynamic modeling and simulation*. Springer, 2011. [citation on page 60]

[14] J. Brown, A. Giaccia. The unique physiology of solid tumors: opportunities (and problems) for cancer therapy. *Cancer Research*, 58:1408–1416, 1998. [citation on page 44]

[15] R. Byrd, R. Schnabel, G. Shultz. A trust region algorithm for nonlinearly constrained optimization. *SIAM Journal on Numerical Analysis*, 24:1152–1170, 1987. [citation on page 61]

[16] J. Campisi. The biology of replicative senescence. *European Journal of Cancer*, 33(5):703–709, 1997. [citation on page 14]

[17] J. Campisi, F. d. di Fagagna. Cellular senescence: when bad things happen to good cells. *Nature Reviews Molecular Cell Biology*, 8(9):729–740, 2007. [citation on page 13]

[18] L. Cesari. *Optimization-theory and applications: problems with ordinary differential equations*, volume 17. Springer-Verlag New York, 1983. [citation on page 48]

[19] Z. Chen, L. C. Trotman, D. Shaffer, H.-K. Lin, Z. A. Dotan, M. Niki, J. A. Koutcher, H. I. Scher, T. Ludwig, W. Gerald, et al. Crucial role of p53-dependent cellular senescence in suppression of Pten-deficient tumorigenesis. *Nature*, 436(7051):725–730, 2005. [citation on page 14]

[20] L. Cheng, H. Zincke, M. L. Blute, E. J. Bergstralh, B. Scherer, D. G. Bostwick. Risk of prostate carcinoma death in patients with lymph node metastasis. *Cancer*, 91(1):66–73, 2001. [citation on page 2]

[21] J. E. Chipuk, D. R. Green. Dissecting p53-dependent apoptosis. *Cell Death and Differentiation*, 13(6):994–1002, 2006. [citation on page 15]

[22] M. Collado, J. Gil, A. Efeyan, C. Guerra, A. J. Schuhmacher, M. Barradas, A. Benguría, A. Zaballos, J. M. Flores, M. Barbacid, et al. Tumour biology: senescence in premalignant tumours. *Nature*, 436(7051):642–642, 2005. [citation on page 14]

[23] R. Cooke. *Dr. Folkman's War: Angiogenesis and the struggle to defeat cancer*. Random House, New York, 2001. [citation on page 44 and 59]

[24] J.-P. Coppé, P.-Y. Desprez, A. Krtolica, J. Campisi. The senescence-associated secretory phenotype: the dark side of tumor suppression. *Annual Review of Pathology*, 5:99–118, 2010. [citation on page 15]

[25] J.-P. Coppé, K. Kauser, J. Campisi, C. M. Beauséjour. Secretion of vascular endothelial growth factor by primary human fibroblasts at senescence. *Journal of Biological Chemistry*, 281(40):29568–29574, 2006. [citation on page 4 and 15]

[26] J.-P. Coppé, C. K. Patil, F. Rodier, Y. Sun, D. P. Muñoz, J. Goldstein, P. S. Nelson, P.-Y. Desprez, J. Campisi. Senescence-associated secretory phenotypes reveal cell-nonautonomous functions of oncogenic RAS and the p53 tumor suppressor. *PLoS Biology*, 6(12):2853–2868, 2008. [citation on page 15]

[27] J. Couzin-Frankel. Cancer immunotherapy. *Science*, 342(6165):1432–1433, 2013. [citation on page 3]

[28] R. Cukier, C. Fortuin, K. E. Shuler, A. Petschek, J. Schaibly. Study of the sensitivity of coupled reaction systems to uncertainties in rate coefficients. i theory. *The Journal of Chemical Physics*, 59(8):3873–3878, 1973. [citation on page 61]

[29] A. R. Davalos, J.-P. Coppe, J. Campisi, P.-Y. Desprez. Senescent cells as a source of inflammatory factors for tumor progression. *Cancer and Metastasis Reviews*, 29(2):273–283, 2010. [citation on page 14]

[30] G. Delaney, S. Jacob, C. Featherstone, M. Barton. The role of radiotherapy in cancer treatment: estimating optimal utilisation from a review of evidence-based guidelines. *Cancer*, 104:1129–1137, 2006. [citation on page 4]

[31] J. Didkowska, U. Wojciechowska. Zachorowania i zgony na nowotowry złośliwe. Krajowy Rejestr Nowotworów, Centrum Onkologii - Instytut im. Marii Skłodowskiej-Curie. http://onkologia.org.pl/k/epidemiologia/. [citation on page 1]

[32] G. P. Dimri, X. Lee, G. Basile, M. Acosta, G. Scott, C. Roskelley, E. E. Medrano, M. Linskens, I. Rubelj, O. Pereira-Smith. A biomarker that identifies senescent human cells in culture and in aging skin in vivo. *Proceedings of the National Academy of Sciences of the United States of America*, 92(20):9363–9367, 1995. [citation on page 21]

[33] M. Dolbniak, A. Świerniak. Comparison of simple models of periodic protocols for combined anticancer therapy. *Computational and Mathematical Methods in Medicine*, 1:1–11, 2013. [citation on page 45]

[34] A. d'Onofrio, A. Gandolfi. Tumour eradication by antiangiogenic therapy: analysis and extensions of the model by Hahnfeldt et al.(1999). *Mathematical Biosciences*, 191:159–184, 2004. [citation on page 28, 29, 50, and 53]

[35] A. d'Onofrio, A. Gandolfi. The response to antiangiogenic anticancer drugs that inhibit endothelial cell proliferation. *Applied Mathematics and Computation*, 181(2):1155–1162, 2006. [citation on page 41 and 72]

[36] A. d'Onofrio, A. Gandolfi. A family of models of angiogenesis and anti-angiogenesis anti-cancer therapy. *Mathematical Medicine and Biology*, 26(1):63–95, 2009. [citation on page 28]

[37] A. d'Onofrio, A. Gandolfi, A. Rocca. The dynamics of tumour–vasculature interaction suggests low-dose, time-dense anti-angiogenic schedulings. *Cell Proliferation*, 42(3):317–329, 2009. [citation on page 41 and 72]

[38] D. Dworakowska. Rola białka p53, prb, p21 waf1/cip1, pcna, mdm2 oraz cykliny d1 w regulacji cyklu komórkowego oraz apoptozy. *Onkologia Polska*, 8(4):223–228, 2005. [citation on page 12]

[39] S. Eckhouse, G. Lewison, R. Sullivan. Trends in the global funding and activity of cancer research. *Molecular Oncology*, 2(1):20–32, 2008. [citation on page 1 and 3]

[40] A. Ergun, K. Camphausen, L. Wein. Optimal scheduling of radiotherapy and angiogenic inhibitors. *Bulletin of Mathematical Biology*, 65:407–424, 2003. [citation on page 27 and 29]

[41] S. C. Erridge, C. Featherstone, R. Chalmers, J. Campbell, D. Stockton, R. Black. What will be the radiotherapy machine capacity required for optimal delivery of radiotherapy in Scotland in 2015? *European Journal of Cancer*, 43(12):1802–1809, 2007. [citation on page 4]

[42] J. A. Ewald, J. A. Desotelle, G. Wilding, D. F. Jarrard. Therapy-induced senescence in cancer. *Journal of the National Cancer Institute*, 102(20):1536–1546, 2010. [citation on page 14]

[43] J. Folkman. Tumor angiogenesis: therapeutic implications. *New England Journal of Medicine*, 18:1182–1184, 1971. [citation on page 3, 16, 40, and 44]

[44] J. Folkman. Angiogenesis in cancer, vascular, rheumatoid and other disease. *Nature Medicine*, 1(1):27–30, 1995. [citation on page 3]

[45] U. Foryś, M. Piotrowska. Analysis of the Hopf bifurcation for the family of angiogenesis models II: the case of two nonzero unequal delays. *Applied Mathematics and Computation*, 220:277–295, 2013. [citation on page 28]

[46] J. S. Fridman, S. W. Lowe. Control of apoptosis by p53. *Oncogene*, 22(56):9030–9040, 2003. [citation on page 13]

[47] J.-E. Frödin, E. Jonsson, T. Möller, L. Werkö. Radiotherapy in Sweden: A study of present use in relation to the literature and an estimate of future trends. *Acta Oncologica*, 35(8):967–979, 1996. [citation on page 4]

[48] K. Fujita, D. Sano, M. Kimura, Y. Yamashita, M. Kawakami, Y. Ishiguro, G. Nishimura, H. Matsuda, M. Tsukuda. Anti-tumor effects of bevacizumab in combination with paclitaxel on head and neck squamous cell carcinoma. *Oncology Reports*, 18(1):47–51, 2007. [citation on page 61, 62, and 66]

[49] M. Greenblatt, W. Bennett, M. Hollstein, C. Harris. Mutations in the p53 tumor suppressor gene: clues to cancer etiology and molecular pathogenesis. *Cancer Research*, 54(18):4855–4878, 1994. [citation on page 13]

[50] C. W. Greider, E. H. Blackburn. Identification of a specific telomere terminal transferase activity in tetrahymena extracts. *Cell*, 43(2):405–413, 1985. [citation on page 13]

[51] P. Hahnfeldt, D. Panigrahy, J. Folkman, L. Hlatky. Tumor development under angiogenic signaling: a dynamical theory of tumor growth, treatment response, and postvascular dormancy. *Cancer Research*, 59:4770–4775, 1999. [citation on page 27, 28, 29, 30, 32, 33, 34, 37, 40, 44, 50, 56, 60, 61, 63, 67, 69, and 72]

[52] D. Hanahan, R. A. Weinberg. The hallmarks of cancer. *Cell*, 100(1):57–70, 2000. [citation on page 14]

[53] D. Hanahan, R. A. Weinberg. Hallmarks of cancer: the next generation. *Cell*, 144(5):646–674, 2011. [citation on page 14]

[54] L. Hayflick, P. S. Moorhead. The serial cultivation of human diploid cell strains. *Experimental Cell Research*, 25(3):585–621, 1961. [citation on page 13]

[55] A. W. Hickman, R. J. Jaramillo, J. F. Lechner, N. F. Johnson. Alpha-particle-induced p53 protein expression in a rat lung epithelial cell strain. *Cancer Research*, 54(22):5797–800, 1994. [citation on page 15]

[56] S. P. Jackson. Sensing and repairing DNA double-strand breaks. *Carcinogenesis*, 23(5):687–696, 2002. [citation on page 12]

[57] R. K. Jain. Normalization of tumor vasculature: an emerging concept in antiangiogenic therapy. *Science*, 307:58–62, 2005. [citation on page 16, 17, 31, and 44]

[58] R. K. Jain. Taming vessels to treat cancer. *Scientific American*, 298:56–63, 2008. [citation on page 16, 17, 31, 44, and 47]

[59] M. Joiner, A. Van der Kogel, G. Steel. *Basic clinical radiobiology*. A Hodder Arnold Publication, London, edition 4th, 2009. [citation on page 12]

[60] J. Klamka, A. Świerniak. Controllability of a model of combined anticancer therapy. *Control and Cybernetics*, 42:125–138, 2013. [citation on page 45]

[61] H. Kondoh, T. Maruyama, M. E. Lleonart. Senescence as a target of cancer therapy. *Open Pathology Journal*, 2:57–62, 2008. [citation on page 13 and 14]

[62] N. Kronik, Y. Kogan, V. Vainstein, Z. Agur. Improving alloreactive CTL immunotherapy for malignant gliomas using a simulation model of their interactive dynamics. *Cancer Immunology, Immunotherapy*, 57(3):425–439, 2008. [citation on page 5]

[63] A. Krtolica, S. Parrinello, S. Lockett, P.-Y. Desprez, J. Campisi. Senescent fibroblasts promote epithelial cell growth and tumorigenesis: a link between cancer and aging. *Proceedings of the National Academy of Sciences of the United States of America*, 98(21):12072–12077, 2001. [citation on page 15]

[64] J. Łanuszewska, P. Widłak. Białka detektorowe rozpoznające pęknięcia nici DNA i ich udział w mechanizmach komórkowej odpowiedzi na stres. *Postępy w Biochemii*, 49(4):229–238, 2003. [citation on page 12]

[65] A. Lasota, M. C. Mackey, M. Ważewska-Czyżewska. Minimizing therapeutically induced anemia. *Journal of Mathematical Biology*, 13(2):149–158, 1981. [citation on page 4]

[66] M. Leach, K. Brindle, J. Evelhoch, J. Griffiths, M. Horsman, A. Jackson, G. Jayson, I. Judson, M. Knopp, R. Maxwell, et al. The assessment of antiangiogenic and antivascular therapies in early-stage clinical trials using magnetic resonance imaging: issues and recommendations. *British Journal of Cancer*, 92(9):1599, 2005. [citation on page 30 and 59]

[67] K. Leder, K. Pitter, Q. LaPlant, D. Hambardzumyan, B. D. Ross, T. A. Chan, E. C. Holland, F. Michor. Mathematical modeling of PDGF-driven glioblastoma reveals optimized radiation dosing schedules. *Cell*, 156(3):603–616, 2014. [citation on page 5]

[68] U. Ledzewicz, H. Schättler. Analysis of optimal controls for a mathematical model of tumour anti-angiogenesis. *Optimal Control Applications and Methods*, 29:41–58, 2008. [citation on page 27, 28, 45, and 57]

[69] U. Ledzewicz, H. Schättler. Optimal and suboptimal protocols for a class of mathematical models of tumor anti-angiogenesis. *Journal of Theoretical Biology*, 252:295–312, 2008. [citation on page 27, 28, 30, 45, and 57]

[70] B. E. Lehnert, E. H. Goodwin, A. Deshpande. Extracellular factor(s) following exposure to alpha particles can cause sister chromatid exchanges in normal human cells. *Cancer Research*, 57(11):2164–2171, 1997. [citation on page 15]

[71] M. E. LLeonart, A. Artero-Castro, H. Kondoh. Senescence induction: a possible cancer therapy. *Molecular Cancer*, 8(3):1–10, 2009. [citation on page 14]

[72] L. Loeb. A mutator phenotype in cancer. *Cancer Research*, 61:3230–3239, 2001. [citation on page 44]

[73] M. D. Lynch. How does cellular senescence prevent cancer? *DNA and Cell Biology*, 25(2):69–78, 2006. [citation on page 14]

[74] E. C. Mackonis, N. Suchowerska, M. Zhang, M. Ebert, D. R. McKenzie, M. Jackson. Cellular response to modulated radiation fields. *Physics in Medicine and Biology*, 52(18):5469–5482, 2007. [citation on page 15]

[75] R. J. Mairs, M. Boyd. National symposium on low-dose radiation and bystander effects -12 October 2004, Cancer Research UK Beatson Laboratories, Glasgow. Sponsored by Glasgow University School for Cancer Studies, the Department of Health and the National Cancer Research Institute. *International Journal of Radiation Biology*, 81(3):259–262, 2005. [citation on page 15]

[76] N. Mantzaris, S. Webb, H. Othmer. Mathematical modeling of tumor-induced angiogenesis. *Journal of Mathematical Biology*, 49(2):111–187, 2004. [citation on page 28]

[77] M. D. McKay, R. J. Beckman, W. J. Conover. Comparison of three methods for selecting values of input variables in the analysis of output from a computer code. *Technometrics*, 21(2):239–245, 1979. [citation on page 61]

[78] E. Michalak, A. Villunger, M. Erlacher, A. Strasser. Death squads enlisted by the tumour suppressor p53. *Biochemical and Biophysical Research Communications*, 331(3):786–798, 2005. [citation on page 13]

[79] W. F. Morgan, M. B. Sowa. Effects of ionizing radiation in nonirradiated cells. *Proceedings of the National Academy of Sciences of the United States of America*, 102(40):14127–14128, 2005. [citation on page 12 and 99]

[80] C. Mothersill, R. G. Bristow, S. M. Harding, R. W. Smith, A. Mersov, C. B. Seymour. A role for p53 in the response of bystander cells to receipt of medium borne signals from irradiated cells. *International Journal of Radiation Biology*, 87(11):1120–1125, 2011. [citation on page 15]

[81] C. Mothersill, C. Seymour. Medium from irradiated human epithelial cells but not human fibroblasts reduces the clonogenic survival of unirradiated cells. *International Journal of Radiation Biology*, 71(4):421–427, 1997. [citation on page 15]

[82] I. H. Mufti. *Computational Methods in Optimal Control Problems*. Springer-Verlag, 1970. [citation on page 53]

[83] C. Nardella, J. G. Clohessy, A. Alimonti, P. P. Pandolfi. Pro-senescence therapy for cancer treatment. *Nature Reviews Cancer*, 11(7):503–511, 2011. [citation on page 14]

[84] M. Piotrowska, U. Foryś. Analysis of the Hopf bifurcation for the family of angiogenesis models. *Journal of Mathematical Analysis and Applications*, 382:180–203, 2011. [citation on page 29]

[85] J. Poleszczuk. Mathematical modelling of tumour angiogenesis. *Mathematica Applicanda*, 41:1–12, 2013. [citation on page 27, 46, 54, 55, and 103]

[86] J. Poleszczuk, M. Bodnar, U. Foryś. New approach to modeling of antiangiogenic treatment on the basis of Hahnfeldt et al. model. *Mathematical Biosciences and Engineering*, 8:591–603, 2011. [citation on page 27, 30, 44, 46, 56, 60, 67, and 69]

[87] J. Poleszczuk, U. Foryś. Derivation of the Hahnfeldt em et al. model (1999) revisited. *Proceedings of the XVI National Conference Applications of Mathematics to Biology and Medicine*, pages 87–92, 2010. [citation on page 27 and 29]

[88] J. Poleszczuk, U. Foryś, M. Piotrowska. New approach to anti-angiogenic treatment modelling and control. *Proceedings of the XVII National Conference Applications of Mathematics to Biology and Medicine*, pages 73–78, 2011. [citation on page 46, 54, 55, and 103]

[89] J. Poleszczuk, P. Hahnfeldt, H. Enderling. Therapeutic implications from sensitivity analysis of tumor angiogenesis models. *PloS one*, 10(3):e0120007, 2015. [citation on page 59]

[90] J. Poleszczuk, A. Krzywoń, U. Foryś, M. Wideł. Connecting radiation-induced bystander effects and senescence to improve radiation response prediction. *Radiation Research*, 183(5):571–577, 2015. [citation on page 4 and 8]

[91] J. Poleszczuk, M. Piotrowska, U. Foryś. Optimal protocols for the anti-VEGF tumor treatment. *Mathematical Modelling of Natural Phenomena*, 9(4):204–215, 2014. [citation on page 43]

[92] J. Poleszczuk, I. Skrzypczak. Tumour angiogenesis model with variable vessels effectiveness. *Applicationes Mathematicae (Warsaw)*, 38(1):33–49, 2011. [citation on page 27 and 45]

[93] L. Pontryagin, V. Boltyanskii, R. Gamkrelidze, E. Mishchenko. *The Mathematical Theory of Optimal Processes*. MacMillan, New York, 1964. [citation on page 48]

[94] L. Preziosi. *Cancer Modelling and Simulation*. CRC Press, 2003. [citation on page 28]

[95] K. M. Prise, O. V. Belyakov, M. Folkard, B. D. Michael. Studies of bystander effects in human fibroblasts using a charged particle microbeam. *International Journal of Radiation Biology*, 74(6):793–798, 1998. [citation on page 15]

[96] C. Robert, J.-C. Soria, A. M. Eggermont. Drug of the year: programmed death-1 receptor/programmed death-1 ligand-1 receptor monoclonal antibodies. *European Journal of Cancer*, 49(14):2968–2971, 2013. [citation on page 3]

[97] F. Rodier, J. Campisi. Four faces of cellular senescence. *The Journal of Cell Biology*, 192(4):547–556, 2011. [citation on page 14]

[98] K. Roszkowski, M. Foksiński. Wpływ promieniowania jonizującego na dna komórki. *Współczesna Onkologia*, 9:284–286, 2005. [citation on page 12]

[99] J. Rzeszowska-Wolny, W. M. Przybyszewski, M. Widel. Ionizing radiation-induced bystander effects, potential targets for modulation of radiotherapy. *European Journal of Pharmacology*, 625(1-3):156–164, 2009. [citation on page 15 and 16]

[100] A. Saltelli, S. Tarantola, K.-S. Chan. A quantitative model-independent method for global sensitivity analysis of model output. *Technometrics*, 41(1):39–56, 1999. [citation on page 63 and 64]

[101] C. A. Schmitt, J. S. Fridman, M. Yang, S. Lee, E. Baranov, R. M. Hoffman, S. W. Lowe. A senescence program controlled by p53 and p16 INK4a contributes to the outcome of cancer therapy. *Cell*, 109(3):335–346, 2002. [citation on page 14]

[102] A. C. Schmitz, M. A. van den Bosch, C. E. Loo, P. T. M. Willem, H. Bartelink, M. Gertenbach, R. Holland, J. L. Peterse, J. T. Emiel, K. G. Gilhuijs, et al. Precise correlation between MRI and histopathology–exploring treatment margins for MRI-guided localized breast cancer therapy. *Radiotherapy and Oncology*, 97(2):225–232, 2010. [citation on page 18]

[103] M. Serrano, M. Blasco. Putting the stress on senescence. *Current Opinion in Cell Biology*, 13(6):748–753, 2001. [citation on page 4 and 13]

[104] M. Serrano, A. W. Lin, M. E. McCurrach, D. Beach, S. W. Lowe. Oncogenic ras provokes premature cell senescence associated with accumulation of p53 and p16 INK4a. *Cell*, 88(5):593–602, 1997. [citation on page 14]

[105] R. L. Siegel, K. D. Miller, A. Jemal. Cancer statistics, 2015. *CA: a Cancer Journal for Clinicians*, 65(1):5–29, 2015. [citation on page 1]

[106] A. Skłodowska, B. Gostkowska. *Promieniowanie jonizujące a człowiek i środowisko*. Wydawnictwo Naukowe Scholar, 1994. [citation on page 11]

[107] B. D. Smith. Imatinib for chronic myeloid leukemia: the impact of its effectiveness and long-term side effects. *Journal of the National Cancer Institute*, 103(7):527–529, 2011. [citation on page 3]

[108] A. C. Society. *Cancer prevention & early detection facts & figures 2012*. Atlanta: American Cancer Society, 2012. [citation on page 2]

[109] P. Sosińska, J. Mikuła-Pietrasik, M. Ryżek, E. Naumowicz, K. Książek. Specificity of cytochemical and fluorescence methods of senescence-associated β-galactosidase detection for ageing driven by replication and time. *Biogerontology*, 15(4):407–413, 2014. [citation on page 21]

[110] G. P. Swanson, I. M. Thompson, J. Basler. Current status of lymph node-positive prostate cancer. *Cancer*, 107(3):439–450, 2006. [citation on page 2]

[111] A. Świerniak. Comparison of six models of antiangiogenic therapy. *Applicationes Mathematicae (Warsaw)*, 36(3):333–348, 2009. [citation on page 27, 28, and 45]

[112] A. Świerniak. Comparison of six models of antiangiogenic therapy. *Applicationes Mathematicae*, 36:333–348, 2009. [citation on page 45]

[113] A. Świerniak. Combined anticancer therapy as a control problem. *Advances in Control Theory and Automation*. Monograph of Committee of Automatics and Robotics PAS, 2012. [citation on page 45]

[114] A. Świerniak. Control problems related to three compartmental model of combined anticancer therapy. *20 IEEE Mediterenian Conference on Automation and Control MED 12, Barcelona*, pages 1428–1433, 2012. [citation on page 45]

[115] A. Świerniak, A. d'Onofrio. Control problems related to tumor angiogenesis. *IEEE Industrial Electronics-IECON2006, Paris, November 6-10*, pages 677–681, 2006. [citation on page 27 and 28]

[116] A. Świerniak, Z. Duda. Singularity of optimal control in some problems related to optimal chemotherapy. *Mathematical and Computer Modelling*, 19:255–262, 1994. [citation on page 57]

[117] A. Świerniak, G. Gala, A. d'Onofrio, A. Gandolfi. Optimization of anti-angiogenic therapy as optimal control problem. *in Proc 4th IASTED Conf. on Biomechanics, ACTA Press (ed. M. Doblaré)*, pages 56–60, 2006. [citation on page 27, 28, and 45]

[118] L. Tartier, S. Gilchrist, S. Burdak-Rothkamm, M. Folkard, K. M. Prise. Cytoplasmic irradiation induces mitochondrial-dependent 53BP1 protein relocalization in irradiated and bystander cells. *Cancer Research*, 67(12):5872–5879, 2007. [citation on page 15]

[119] J. Thariat, J. Hannoun-Levi, A. S. Myint, T. Vuong, J.-P. Gérard. Past, present, and future of radiotherapy for the benefit of patients. *Nature Reviews Clinical Oncology*, 10(1):52–60, 2013. [citation on page 4]

[120] P. Thorpe. Vascular targeting agents as cancer therapeutics. *Clinical Cancer Research*, 10(2):415–427, 2004. [citation on page 30]

[121] T. D. Tlsty. Functions of p53 suppress critical consequences of damage and repair in the initiation of cancer. *Cancer Cell*, 2(1):2–4, 2002. [citation on page 15]

[122] M. Tomita, M. Maeda, K. Kobayashi, H. Matsumoto. Dose response of soft X-ray-induced bystander cell killing affected by p53 status. *Radiation Research*, 179(2):200–207, 2013. [citation on page 16]

[123] L. A. Torre, F. Bray, R. L. Siegel, J. Ferlay, J. Lortet-Tieulent, A. Jemal. Global cancer statistics, 2012. *CA: a Cancer Journal for Clinicians*, 65(2):87–108, 2015. [citation on page 1, 2, 3, and 99]

[124] R. E. Vatner, B. T. Cooper, C. Vanpouille-Box, S. Demaria, S. C. Formenti. Combinations of immunotherapy and radiation in cancer therapy. *Frontiers in Oncology*, 4(325):1–15, 2014. [citation on page 4]

[125] O. von Stryk, R. Bulirsch. Direct and indirect methods for trajectory optimization. *Annals of Operation Research*, 37(1):357–373, 1992. [citation on page 53]

[126] C. Wu, J. van Riggelen, A. Yetil, A. C. Fan, P. Bachireddy, D. W. Felsher. Cellular senescence is an important mechanism of tumor regression upon c-myc inactivation. *Proceedings of the National Academy of Sciences of the United States of America*, 104(32):13028–13033, 2007. [citation on page 14]

[127] M. Xin, J. Zhang, E. R. Block, J. M. Patel. Senescence-enhanced oxidative stress is associated with deficiency of mitochondrial cytochrome c oxidase in vascular endothelial cells. *Mechanisms of Ageing and Development*, 124(8):911–919, 2003. [citation on page 15]

[128] J. Yang, L. Haworth, R. Sherry, P. Hwu, D. Schwartzentruber, S. Topalian, S. Steinberg, H. Chen, S. Rosenberg. A randomized trial of bevacizumab, an anti-vascular endothelial growth factor antibody, for metastatic renal cancer. *The New England Journal of Medicine*, 349(5):427–434, 2003. [citation on page 31]

[129] A. R. Young, M. Narita. SASP reflects senescence. *EMBO Reports*, 10(3):228–230, 2009. [citation on page 15]

Appendices

Appendix A

Numerical procedures

A.1 Numerical procedures used for optimal protocol estimation

Table of Contents

main

```
function main()
%MAIN FUNCTION FOR OPTIMAL CONTROL SEARCH

addpath('Additional functions');
addpath('Core functions');
addpath('Models');
addpath('Plot functions');

%%%%--- INITIALIZE ---%%%%
%%%% Setting all necessary parameters

    [par, init,u]=initSettings();

    [S, I, dS, dI] = selectModel(par.model);

%%%%--- ---%%%%

%%%%--- CALCULATING INITIAL SOLUTION AND PAYOFF ---%%%%

    solM=solveModel( S,I,u, par, init);
    Jinit=payoff(solM.y(1,end),solM.y(2,end),u,par);


%%%%--- --- %%%%

%%%%--- GRADIENT BASED METHOD ---%%%%
%%%% Finding initial guess for shooting method

    %display('Starting gradient method...');
    niter=1; JPrev=1e10; JTmp=Jinit;

    while abs(JPrev-JTmp)>par.gradTol

        JPrev=JTmp;
```

```
            solC=solveCostateInv(solM,u, dS, dI, par);
            [tmesh, ~, dHu]=Hamiltonian(solM,solC,u,S,I,par);

            [l1, u] = findOpt(u, dHu, tmesh, S, I, par, init);

            solM=solveModel(S, I, u, par, init);
            JTmp=payoff(solM.y(1,end),solM.y(2,end),u,par);

            %display(['J value after ' num2str(niter) ...
            %         'iterations:' num2str(JTmp)]);
            niter=niter+1;
        end

        %display('Tolerance met - stopping.');
        %display('_____________________________');

    %%%%--- ---%%%%

    %%%%--- SHOOTING METHOD ---%%%%
    %%%% Finding optimal control with shooting method

        %display('Starting shooting method...');

        [x0, val, uN] = findOptShooting( S, I, dS, dI, par, init, u );

        %display('_____________________________');

    %%%%--- ---%%%%

    %%%%--- DISPLAY FINAL RESULT ---%%%%
    %%%% Display final procedure report

        solMFinal=solveModel( S,I,uN, par, init);

        JFinal=payoff(solMFinal.y(1,end),solMFinal.y(2,end),uN,par);

        %display(['Final J value: ' num2str(JFinal)]);
        %display(['Shooting method error: ' num2str(val)]);

    %%%%--- ---%%%%

    %%%%--- PLOT SOLUTION ---%%%%
    %%%% Plot respective solution components

        %plotControl(solMFinal,uN,[0.63 0.5 0.25 0.25],1);

    %%%%--- ---%%%%
    end
```

initSettings

```
    function [params, init, u] = initSettings()
```

```
        %%%%--- MODEL ASSOCIATED PARAMETERS ---%%%%

        params.model='Ergun'; %{'Hahnfeldt', 'Ergun', 'dOnofrio'}

        params.angType=1;  %0 -> original model, 1 -> modified model

        params.eps=0.2032; %tumor growth rate: -eps*p*log(p/q)
        params.mu=0;       %spontaneous loss of vasculature: -mu*q
        params.d=0.0028;   %endogenous inhibition: -d*I(p,q)
        params.l=10.3915;  %stimulation: l/(a+u(t))*S(p,q)
        params.a=4.5980;   %stimulation: l/(a+u(t))*S(p,q)
        params.e=0.0273;   %drug influence: -e*u(t)*q

        init=[2000; 3000]; %initial condition (p(0),q(0))

        params.Tmax=30;    %final time

        %%%%--- ---%%%%


        %%%%--- OPTIMAL CONTROL PROBLEM SETTINGS ---%%%%

        params.Ub=20;    %upper bound for control
        params.Lb=0;     %lower bound for control

        params.k1=2;     %payoff functional parameter: k1*Integrate(u(t))
        params.k2=1000;  %payoff functional parameter: -k2*q(T)/p(T)

        %%%%--- ---%%%%

        %%%%--- SOLVER SETTINGS ---%%%%

        %initial control
        u.ti=[0 params.Tmax];
        u.ui=[params.Ub params.Ub];

        params.gradTol=1e-0; %tolerance for the gradient method

        params.solTol=1e-8;  %RelTol for the ode methods

        %%%%--- ---%%%%

    end
```

Hamiltonian

```
    function [tmesh, H, dHu] = Hamiltonian(solM,solC,u,S,I,par)
    %HAMILTONIAN - function calculating Hamiltonian value and value of its
    %derivative with respect to control u

    H=NaN; %no need to calculate in this version of the code
```

```
tmesh=unique([solM.x solC.x]);
solMm=deval(solM,tmesh);
solCc=deval(solC,tmesh);

if par.angType
    dHu=par.k1-par.l./(par.a+control(tmesh,u)).^2.*solCc(2,:).*...
        feval(S,solMm(1,:),solMm(2,:));
else
    dHu=par.k1-par.e*solCc(2,:).*solMm(2,:);
end


end
```

control

```
function u = control(t,ms)
    %return value of the control at time t
    u=interp1(ms.ti,ms.ui,t);
end
```

findOpt

```
function [l1, uN] = findOpt(u,dHu,tmesh,S,I,par, init)
%FINDOPT - function finding the best value by which multiply the
%Hamiltonians derivative and add to control.

    %%%% creating common mesh and taking values
    tmeshN=unique([u.ti tmesh]);
    uN=interp1(u.ti,u.ui,tmeshN);
    dHuN=interp1(tmesh,dHu,tmeshN);

    u.ti=tmeshN;
    u.ui=uN;

    %%%%

    for i=1:10
        options = optimset('Display','none');
        l1=abs(fminsearch(@F,i,options));
        if F(l1)<F(0)
            uN=u;
            uN.ui=min(max(u.ui-l1*dHuN,par.Lb),par.Ub);
            break;
        end
    end

    if F(l1)>=F(0)
        l1=0;
        uN=u;
    end

    function y=F(x)
```

```
            ux=u;
            ux.ui=min(max(u.ui-abs(x)*dHuN,par.Lb),par.Ub);
            solM=solveModel( S, I, ux, par, init);
            y=payoff(solM.y(1,end), solM.y(2,end), ux, par);
        end

    end
```

findOptShooting

```
    function [x0, val, uout] = findOptShooting( S, I, dS, dI, par, init, u )
    %FINDOPTSHOOTING - function approximating the optimal control using
    %shooting method.

        solMinit=solveModel( S,I,u, par, init);
        solCinit=solveCostateInv(solMinit,u, dS, dI, par);

        initC=deval(solCinit,0);

        options=optimset('Display','none','TolX',1e-10,'TolFun',1e-10);
        [x0, val]=lsqnonlin(@F, initC,[],[],options);

        [~, uout]=F(x0);

        function [y, u]=F(x)

            solM=solveFullSystem( S,I, dS, dI, par, [init; x]);

            u.ti=solM.x;
            u.ui=solveHu(solM.x,solM.y,S,par);

            [~,bound]=payoff(solM.y(1,end),solM.y(2,end),u,par);

            y=solM.y(3:4,end)-bound;
        end
    end
```

payoff

```
    function [J, Mdx]= payoff(p,q,u,par)
    %PAYOFF - function returning value of the payoff functional and
    %corresponding terminal conditions for the adjoint equations.

    J=p+par.k1*trapz(u.ti,u.ui)-par.k2*q/p;

    Mdx=[1+par.k2*q/p^2; -par.k2/p];

    end
```

solveCostateInv

```
    function solC = solveCostateInv( sPQ,u, dS, dI, par  )
```

```
%SOLVECOSTATEINV - solving adjoint equations backward in time.

    [~,init]=payoff(sPQ.y(1,end),sPQ.y(2,end),u,par);

    options=odeset('RelTol',par.solTol,'Refine',10);

    if par.angType
        solC=ode45(@costateEqns,[par.Tmax 0],init,options);
    else
        solC=ode45(@costateEqnsClassic,[par.Tmax 0],init,options);
    end


    function dY=costateEqns(t,y) %adjoint equations for modified model
        dY=zeros(2,1);
        pq=deval(sPQ,t);
        w=par.l/(par.a+control(t,u));
        vdS=feval(dS,pq(1),pq(2));
        vdI=feval(dI,pq(1),pq(2));

        dY(1)=par.eps*y(1)*(log(pq(1)/pq(2))+1)-...
              y(2)*(w*vdS(1)-par.d*vdI(1));
        dY(2)=-par.eps*y(1)*pq(1)/pq(2)+...
              y(2)*(par.mu-w*vdS(2)+par.d*vdI(2));
    end

    function dY=costateEqnsClassic(t,y) %adjoint eqs for original model
        dY=zeros(2,1);
        pq=deval(sPQ,t);
        w=control(t,u);
        vdS=feval(dS,pq(1),pq(2));
        vdI=feval(dI,pq(1),pq(2));

        dY(1)=par.eps*y(1)*(log(pq(1)/pq(2))+1)-...
              y(2)*(par.l/par.a*vdS(1)-par.d*vdI(1));
        dY(2)=-par.eps*y(1)*pq(1)/pq(2)+...
              y(2)*(par.mu-par.l/par.a*vdS(2)+par.d*vdI(2)+par.e*w);
    end
end
```

solveFullSystem

```
function solM = solveFullSystem( S, I, dS, dI, par, init)

    options=odeset('RelTol',1e-10);

    if par.angType
        solM=ode45(@vectField,[0 par.Tmax],init,options);
    else
        solM=ode45(@vectFieldClassic,[0 par.Tmax],init,options);
    end

    function dY=vectField(t,x)
```

```
            u=solveHu(t,x,S,par);
            w=par.l/(par.a+u);

            dY=zeros(4,1);
            dY(1)=-par.eps*x(1)*log(x(1)/x(2));
            dY(2)=-par.mu*x(2)-par.d*feval(I,x(1),x(2))+...
                  w*feval(S,x(1),x(2));

            vdS=feval(dS,x(1),x(2));
            vdI=feval(dI,x(1),x(2));


            dY(3)=par.eps*x(3)*(log(x(1)/x(2))+1)-...
                  x(4)*(w*vdS(1)-par.d*vdI(1));
            dY(4)=-par.eps*x(3)*x(1)/x(2)+...
                  x(4)*(par.mu-w*vdS(2)+par.d*vdI(2));
        end

        function dY=vectFieldClassic(t,x)
            w=solveHu(t,x,S,par);%control(t,u0);

            dY=zeros(4,1);
            dY(1)=-par.eps*x(1)*log(x(1)/x(2));
            dY(2)=-par.mu*x(2)-par.d*feval(I,x(1),x(2))+...
                  par.l/par.a*feval(S,x(1),x(2))-w*par.e*x(2);

            vdS=feval(dS,x(1),x(2));
            vdI=feval(dI,x(1),x(2));

            dY(3)=par.eps*x(3)*(log(x(1)/x(2))+1)-...
                  x(4)*(par.l/par.a*vdS(1)-par.d*vdI(1));
            dY(4)=-par.eps*x(3)*x(1)/x(2)+...
                  x(4)*(par.mu-par.l/par.a*vdS(2)+par.d*vdI(2)+par.e*w);
        end

    end
```

solveHu

```
    function u = solveHu(~,x,S,par)

        if par.angType

            u=(x(4,:).*feval(S,x(1,:),x(2,:))<=0)*par.Lb+...
              (x(4,:).*feval(S,x(1,:),x(2,:))>0).*...
              max(min(abs(sqrt(1./(par.k1./x(4,:)./...
              feval(S,x(1,:),x(2,:))/par.l)))-par.a,par.Ub),par.Lb);

        else

            u=((par.k1-par.e.*x(4,:).*x(2,:))>0)*par.Lb+...
              ((par.k1-par.e.*x(4,:).*x(2,:))<=0)*par.Ub;
```

```
    end

end
```

solveModel

```
function solM = solveModel( S,I,u, par, init )
%SOLVEMODEL - function returning solution to the model specified by the
%S(p,q) and I(p,q) function with the parameters in par.

    options=odeset('RelTol',par.solTol,'Refine',10);

    if par.angType
        solM=ode45(@vectField,[0 par.Tmax],init,options);
    else
        solM=ode45(@vectFieldClassic,[0 par.Tmax],init,options);
    end

    function dY=vectField(t,x) %vector field for the modified model
        dY=zeros(2,1);
        dY(1)=-par.eps*x(1)*log(x(1)/x(2));
        dY(2)=-par.mu*x(2)-par.d*feval(I,x(1),x(2))+...
              par.l/(par.a+control(t,u))*feval(S,x(1),x(2));
    end

    function dY=vectFieldClassic(t,x) %vector field for the original model
        dY=zeros(2,1);
        dY(1)=-par.eps*x(1)*log(x(1)/x(2));
        dY(2)=-par.mu*x(2)-par.d*feval(I,x(1),x(2))+...
              par.l/par.a*feval(S,x(1),x(2))-control(t,u)*par.e*x(2);
    end

end
```

selectModel

```
function [S, I, dS, dI] = selectModel( model )
%SELECTMODEL - function returning handles to the functions defining the
%respective models (I(p,q) and S(p,q)) together with the Jacobi matrix D[I,
%S]. Defined models: 'Hahnfeldt', 'Ergun', 'dOnofrio'.

    switch model
        case 'Hahnfeldt'
            S=@(p,q)(p);
            I=@(p,q)(q.*p.^(2/3));
            dS=@(p,q)([1; 0]);
            dI=@(p,q)([2/3*q.*p.^(-1/3); p.^(2/3)]);
        case 'Ergun'
            S=@(p,q)(q.^(2/3));
            I=@(p,q)(q.^(4/3));
            dS=@(p,q)([0; 2/3*q.^(-1/3)]);
            dI=@(p,q)([0; 4/3*q.^(1/3)]);
        case 'dOnofrio'
```

```
            S=@(p,q)(q);
            I=@(p,q)(q.*p.^(2/3));
            dS=@(p,q)([0; 1]);
            dI=@(p,q)([2/3*q.*p.^(-1/3); p.^(2/3)]);
    end

end
```

Published with MATLAB® R2013b

List of Figures

List of Tables